EXPERIMENTAL STUDY OF THE VAPORIZATION OF CRYOGENIC LIQUIDS ON SOLID SUBSTRATES

A Thesis

by

ASMA SADIA

Submitted to the Office of Graduate and Professional Studies of
Texas A&M University
in partial fulfillment of the requirements of the degree of

MASTER OF SCIENCE

Chair of Committee,	Luc Véchot
Co-Chair of Committee,	Sam Mannan
Committee Member,	Eyad Masad
Head of Department,	M. Nazmul Karim

May 2015

Major Subject: Chemical Engineering

ABSTRACT

Many safety challenges are associated with the production, handling and transportation of Liquefied Natural Gas (LNG) due to its hazardous properties and nature that is significantly different than any other hydrocarbons, namely very low temperature. One such challenge includes prediction of the vaporization rate of LNG during the potential loss of containment. The vaporization rate is vital for the assessment of the risk associated with such event and their mitigation. The present work focuses on the contribution of conductive heat flux on the vaporization rate of cryogens. A series of small-scale, laboratory experiments were designed to carry out the spill of cryogenic liquids on solid substrates. The effects of type of cryogenic liquid (pure or binary mixture), type of solid substrate (concrete or steel) and surface roughness on the vaporization rate of the cryogens were studied.

Three boiling regimes, film, transition and nucleate, were observed during the experiments. The effect of surface roughness was observed to be in agreement with that of non-cryogenic liquids. The effect of mixture composition on its boiling rate were in good agreement with the experimental data available for cryogen spill on water.

Obtained experimental data were used to validate couple of predictive mathematical models, namely 1D ideal conduction through semi-infinite solid and film/nucleate boiling regimes model. Both models did not represent experimental data well and they need severe improvement to be able to predict the complete boiling process.

DEDICATION

This thesis is dedicated to Allah Almighty who has been my eternal rock and source of refuge. I also dedicate this work to my parents, Nasima and Mohd. Abu Taher Chowdhury and my brother, Shadman Shakib Chowdhury for their constant love, prayers and support. My dedication will be incomplete without mentioning my Grandfather, Mohd. Nurul Islam, who has believed in me and has always wished me success in every sphere of life.

ACKNOWLEDGEMENTS

I would like to express the deepest appreciation to my advisor, Dr. Luc Véchot, who has guided me in my research work and provided me with valuable advice for my future endeavors. I would like to acknowledge my committee members: Dr. Sam Mannan and Dr. Eyad Masad. I want to thank Dr. Tomasz Olewski, whose support was instrumental in the completion of my work.

I would also like to appreciate the support of all members of Mary Kay O'Connor Process Safety Center at Qatar. I want to acknowledge the financial and material support provided by Qatar National Research Fund (a member of Qatar Foundation) and Qatar Petroleum.

NOMENCLATURE

Latin Letters

A	Surface area of the substrate that is in contact with the liquid pool, m^2
C_p	Specific heat capacity, J K^{-1}
f	Averaged fraction of the surface in contact with liquid at a given time
g	Gravitational acceleration, m s^{-2}
h	Height of the liquid in the box, m
k	Thermal conductivity of the substrate, W m^{-1} K^{-1}
l	Side length of the substrate, m
m	Mass, kg
n_i	Number of moles of component I, moles
q	Heat flux, W m^{-2}
T	Temperature, K
t	Time, s
T_b	Boiling temperature of the liquid, K
T_i	Initial temperature of the substrate and temperature at infinite depth, K
T_s	Saturation temperature of the liquid, K
V	Vaporization rate due to conduction, kg s^{-1}
v	Kinematic viscosity of the liquid, m^2 s^{-1}
V_i	Concentration of component i, %v/v
z	Distance measured downwards from the surface of the ground, m
ΔT	Temperature difference, K
ΔT^*	Dimensionless temperature difference

Greek Letters

α	Thermal diffusivity of the substrate, m^2 s^{-1}
λ	Latent heat of vaporization, J g^{-1}

ρ	Density, kg m^{-3}
ρ_i	Density of component i, kg m^{-3}
σ	Surface tension, N m^{-1}

Subscripts

b	Base of the box
c	Critical point
cond	Conduction
Cr	Critical heat flux point
f	Film boiling
i	Initial
l	Liquid
min	Leidenfrost point
n	Nucleate boiling
t	Transition
vf	Vapor film
vs	Saturated vapor
w	Wall
wb	Walls and base of the box

Abbreviation

1D	One-Dimensional
ALARP	As Low As Reasonably Practicable
CHF	Critical Heat Flux
GAO	Government Accountability Office
GC	Gas Chromatography
HSL	Health and Safety Laboratory
LFL	Lower Flammability Limit
LN_2	Liquid Nitrogen

LN_2/O_2	Liquid Nitrogen/Oxygen mixture
LNG	Liquefied Natural Gas
MKOPSC-Q	Mary Kay O'Connor Process Safety Center at Qatar
ONB	Onset to Nucleate Boiling
VLE	Vapor Liquid Equilibrium

TABLE OF CONTENTS

Page

ABSTRACT ii

DEDICATION iii

ACKNOWLEDGEMENTS iv

NOMENCLATURE v

TABLE OF CONTENTS viii

LIST OF FIGURES x

LIST OF TABLES xiii

1. INTRODUCTION 1

2. LITERATURE REVIEW 5

2.1 Simple approach: 1D conduction model 7
2.2 Pool boiling phenomena 10
2.2.1 Film boiling 11
2.2.2 Nucleate boiling 13
2.2.3 Transition boiling 15
2.2.4 Modeling of boiling regimes 15
2.2.5 Effect of surface roughness on boiling 19
2.2.6 Effect of chemical composition on boiling 22
2.3 Experimental study of the boiling of cryogenic liquid in the published literature 27
2.4 Bridging the gaps in the literature 30

3. SCOPE OF WORK 32

4. METHODOLOGY 35

4.1 Determination of vaporization rate and conductive heat flux 38
4.2 Comparison with models 39
4.2.1 Thermal properties of solid substrate 40
4.2.2 1D semi-infinite solid, “ideal” conduction model 41

4.2.3 Boiling regimes model 42

5. EXPERIMENTAL SETUP 44

5.1 Concrete base 44
5.2 Steel base 48
5.3 Polystyrene base 49
5.4 Thermal properties of concrete 50
5.5 Challenges encountered 53

6. RESULTS AND ANALYSIS 54

6.1 The effect of concrete surface roughness on vaporization rate of liquid nitrogen and the validation of models 56
6.2 The effect of type of solid substrate (concrete and steel) on the vaporization rate of liquid nitrogen 63
6.3 Binary mixture effect on smooth concrete 66
6.4 The determination of the transition from boiling to evaporation regime of cryogenic liquid spilled on solid substrate 71

7. CONCLUSION AND FUTURE WORK 73

REFERENCES 76

APPENDIX 81

LIST OF FIGURES

Page

Figure 1: Heat transfer process during the pool vaporization of a cryogenic liquid on a solid substrate.....6

Figure 2: Boiling curve (Nukiyama, 1934) [15] 11

Figure 3: Photograph of film boiling regime of liquid nitrogen [17].....12

Figure 4: Photograph of nucleate boiling regime of liquid nitrogen [17] 13

Figure 5: Photograph of transition boiling regime of liquid nitrogen [17] 15

Figure 6: Effect of surface roughness on the boiling curve of pentane on copper [24].....20

Figure 7: Effect of surface roughness on the boiling curve of pentane on Inconel [24].....21

Figure 8: Effect of surface roughness on the boiling curve of water [32].....22

Figure 9: Phase equilibrium diagram of methane-ethane binary system [34].....23

Figure 10: Boiling temperature of LNG and mole fraction of methane in the liquid phase with time [34].....24

Figure 11: Schematic diagram depicting the principle changes to pool boiling curve for binary mixture [35].....25

Figure 12: Schematic of methodology 36

Figure 13: Schematic of general experimental setup 37

Figure 14: A typical mass measurement during the experiment.....38

Figure 15: A typical curve obtained for heat flux provided to the pool as a function of time using 1D conduction model.....42

Figure 16: Heat flux to the pool vs. time curve generated from the boiling curve 43

Figure 17: Rough/smooth surface concrete base setup (H1-H3 are the heat flux sensors and T1-T8 are the thermocouples; all dimensions mentioned in mm) 45

Figure 18: A photograph of smooth surface concrete slab covered with rocks 47

Figure 19: Steel base setup (H1 is the heat flux sensor and T1-T8 are the thermocouples; all dimensions mentioned in mm).....48

Figure 20: Polystyrene setup (H1-H3 are the heat flux sensors; T1-T17 are the thermocouples; all dimensions mentioned in mm).....50

Figure 21: Thermal conductivity and heat capacity of used concrete as a function of temperature 51

Figure 22: Variable thermal conductivity of concrete with temperature and water content [49,50] 52

Figure 23: Variable specific heat capacity of concrete with temperature [49] 52

Figure 24: Repeatability of LN_2 experiments on rough concrete surface 56

Figure 25: Repeatability of LN_2 experiments on smooth concrete surface.....57

Figure 26: Temperature profile in the concrete setup at different depths (from the boiling surface) and pool temperature during LN2 spill on concrete 58

Figure 27: Comparison of rough and smooth surface concrete experiments with the 1D and boiling regimes model 62

Figure 28: Repeatability of LN_2 experiments on steel plate 64

Figure 29: Temperature profile in the steel setup at different depths (from the boiling surface) and pool temperature during LN_2 spill on steel 66

Figure 30: Repeatability of LN_2/O_2 experiments on smooth concrete surface 67

Figure 31: Pool temperature during LN_2/O_2 spill on smooth surface concrete.....68

Figure 32: Mass vaporized of pure and binary mixture on smooth surface concrete 69

Figure 33: The vaporization of pure and binary mixture on smooth surface concrete 70

Figure 34: Pool temperature vs time at different wind speeds during the polystyrene base experiment 72

Figure 35: Experimental setup for rough surface concrete base in the lab 96

Figure 36: Engineering drawing of Steel base set up - bottom view where the depth is mentioned below the thermocouple label (All dimensions mentioned in mm) 98

Figure 37: Risk Matrix 103

LIST OF TABLES

Page

Table 1: Previous notable experimental work on cryogenic liquid boiling 28

Table 2: Thermal properties of concrete at T_i and T_b 41

Table 3: Composition of concrete 46

Table 4: Surface roughness of concrete base setup 46

Table 5: List of total runs conducted for each experiment and their status 55

Table 6: CHF and Leidenfrost values of boiling of LN2 on smooth and rough surface concrete 63

Table 7: CHF and Leidenfrost values of boiling of LN_2 and LN_2/O_2 on smooth surface concrete 71

Table 8: History of accidents at LNG industry [5,6,52] 82

Table 9: Antoine parameter for oxygen and nitrogen [53] 90

Table 10: Surface roughness measurements for rough concrete 95

Table 11: Sensor location in the rough and smooth surface concrete base setups 97

Table 12: Sensor location in the steel base setup 99

Table 13: Sensor location in the polystyrene base setup 100

Table 14. Likelihood of the event 101

Table 15. Severity of the consequences 102

Table 16. Risk acceptance criteria 104

Table 17: What-if Analysis 105

Table 18: Checklist before the experiment 116

1. INTRODUCTION

The world global demand for ecological and clean alternative energy is currently growing. Natural gas has proven to be a source of energy that meets this requirement. It accounted for a share of 23.7% in the global energy consumption in 2013. In the same year, the global natural gas production and consumption grew by 1.1% and 1.4% respectively [1].

In many cases, transportation of natural gas by pipelines is not a practical nor an economically viable option. A better option, particularly in the case of transportation over long distances, is to liquefy natural gas and transport it as Liquefied Natural Gas (LNG). This liquefaction of natural gas provides a 600 fold reduction in volume [2].

Qatar has played a key role in the LNG business. In 2013, Qatar's production of LNG has increased by 5.4%. In the same year, the global natural gas trade increased by 1.8% and the global LNG trade improved by 0.6%. Qatar, being the largest LNG exporter, accounted for about 32% of the global LNG exports and helped in achieving the highest global trade growth increment of 2.7% [1].

LNG is a liquefied hydrocarbon mixture mainly composed of methane (>85%), and C_{2-4} hydrocarbon and Nitrogen in smaller proportions [3]. The boiling point of LNG is -161 °C and hence it is classified as a cryogen [4]. The flammability limits of LNG vapor is 5 % - 15 % [5].

Many safety challenges are associated with the production, handling and transportation of LNG due to its hazardous nature. The LNG industry has a relatively good

safety performances over the last decades compared to other oil and gas industries. However, the accidents that have been reported (Section 0) demonstrated that major incidents involving LNG can lead to very serious consequences. The most deadly accident happened in 1944 in Cleveland, Ohio, USA where a LNG tank failed catastrophically leading to a major loss of containment of LNG followed by fire and explosion. This accident resulted in 124 fatalities and more than 200-400 injuries besides very significant damages to the assets. In 2014, two LNG tankers collision were reported, one of them involving Qatar Gas-owned LNG tanker Al Gharrafa [6]. While these collisions did not lead to the loss of containment of LNG they showed that such catastrophic major event remain possible.

One significant safety challenge resides in the prevention of accidental spill of LNG on ground or water and the mitigation of the associated consequences. Indeed, the spill of cryogenic LNG on ground or water will lead to vigorous vaporization of the liquid which will lead to formation of a flammable LNG vapor cloud that will disperse downwind. If this cloud, within its flammable range, meets an ignition source, fire or explosion may occur, possibly severely affecting employees, public, assets and business. The control of the risks associated to such events a level that is As Low As Reasonably Practicable (ALARP) are of crucial importance for the safety and durability of the LNG industry and therefore energy security.

The assessment of the risks associated to the loss of containment of LNG requires the estimation of their likelihood and the severity of their consequences. The estimation of the severity of the consequences of such events itself requires the prediction of the LNG

vapor production rate, referred to as *source term*, following an accidental spill and the dispersion of the flammable vapor. While, significant research effort has been spent on the development and validation of LNG vapor dispersion models over the past thirty years [4], regrettably much less effort was spent on the development and experimental validation of source term models. This lack of extensive research on source term modelling has been highlighted in a report prepared by the US Government Accountability Office (GAO) in 2007, in which a panel of 19 experts on the topic listed a number of LNG safety related research areas requiring improvement [7]. Another report prepared by the UK Health and Safety Laboratory (HSL) in 2010 stressed the current lack of published research on the development and validation of source term models for LNG spills on land and water. The HSL report also stated that the absence of research in source term modeling could be due to the complexity and variability associated with collecting experimental data close to the source. It also draws attention to the urgent need for good quality experimental data to validate the existing source term models rate.

The improvement of our capability to assess the source term (LNG vaporization rate), following a loss of containment of LNG, is vital for the assessment of the risks associated to such event and their control. Indeed, any uncertainties in the source term modelling have a direct impact on the results of the dispersion modelling (thus the size of the hazardous zone generated by the spill), the overall assessment of the consequences of the spill and ultimately the quality of the risk assessment performed for a given facility [4].

The research performed in this thesis is a part of a global effort to fill the gaps in LNG source term modeling identified by GAO and HSL. The objective of this research

work is to perform the experimental study of the vaporization of a cryogenic liquid when spilled on land. This thesis focuses on the assessment of the consequences of a LNG spill on a solid substrate, and in particular, in the evaluation of the rate of vaporization of LNG pool, referred to as *Source Term* [4], that is used as an input data for the vapor dispersion modelling and subsequently the assessment of the risks associated to the loss of containment of LNG. The prediction of the LNG vapor dispersion is out of the scope of this thesis.

The main focus of the work presented in the thesis will be on the contribution of conductive heat flux on the vaporization rate of the liquid, as the liquid pool undergoes different boiling regimes (film, transition and nucleate regimes) during its lifetime. The effect of the type of cryogenic liquid (pure or binary mixtures), type of solid substrate and surface roughness on the vaporization rate will be studied. The experimental results will then be compared to existing source term models currently being used in the commercial software for consequence modeling. Part of the research will also look at the possibility of evaporative cooling during the spill on a solid substrate.

2. LITERATURE REVIEW

The prediction of *source term* for a spill of LNG on land requires the understanding of the physical phenomena governing the vaporization of cryogenic liquids (or cryogen[*]) when spilled on a solid substrate initially at ambient temperature.

When a cryogenic liquid is accidentally released on land (for instance following the catastrophic failure of a vessel, the rupture of a pipeline carrying cryogen or a jet of liquid impacting a solid surface), the liquid will form a spreading pool on the ground. This spreading liquid pool boils vigorously as a result of heat transfer between the pool and the surroundings. The pool boiling rate depends on rate of heat transfer to the liquid, the composition of the pool and the surface area of the pool [4]. Figure 1 illustrates the heat transfer mechanisms involved in the pool ***boiling*** [8]:

Conduction: Conduction from the solid substrate to the liquid pool was shown to be the prevailing heat transfer mechanism particularly at the initial stages of spill [4,7] when the temperature difference between the substrate (initially at ambient temperature) and the pool is large. Conductive heat transfer will cause the substrate to cool down more or less rapidly depending on the thermal properties of this substrate.

Convection: Convective heat transfer from the air to the liquid pool contribute to the total heat input into the liquid pool. The relative contribution of convection to the total heat transfer rate is negligible at the early stage of the spill (compared to conduction).

[*] Cryogenic liquid refers to liquids that boils at a temperature below -150°C at atmospheric pressure [54], such as LNG ($T_{boiling}$ = -162°C).

Vechot *et al.* [9] showed that convection play a more significant and non-negligible role in the overall vaporization rate as the ground cools down.

Radiation from the sun: Solar radiation may count for less than 5 % of the total heat gained by the cryogenic pool [5] and is often ignored.

Radiation from tan adjacent fire: Thermal radiation gained from an adjacent may significantly increase the pool boiling rate.

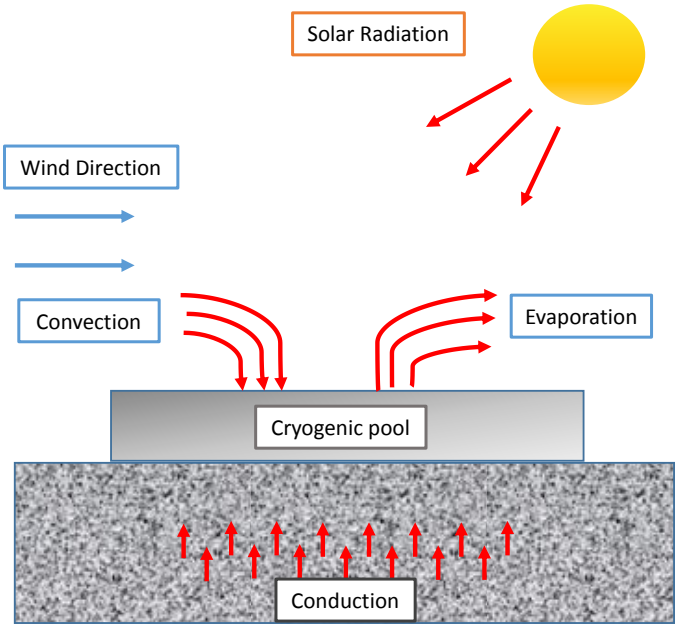

Figure 1: Heat transfer process during the pool vaporization of a cryogenic liquid on a solid substrate

As the ground cool down the combined heat transfer contributions from conduction, convection and radiation may not be sufficient to sustain pool boiling. In this case, evaporation (surface vaporization of the liquid) may cause the cooling of the pool

below its boiling point. This phenomena is referred to as evaporative cooling. The overall vaporization rate will then be governed by the pool evaporation rate.

The focus of this thesis will be the study of pool boiling by conduction. An attempt will be made to study the possibility of evaporative cooling during the pool vaporization process.

The effect of convective and radiative heat transfer mechanisms are simultaneously being investigated by the Mary Kay O'Connor Process Safety Center – Qatar and is not within the scope of this thesis.

2.1 Simple approach: 1D conduction model

The simplest and widely used [10,11] approach for the modelling of the conductive heat transfer from the ground was developed using the following assumptions [4,10,12]:

- Heat conduction is one dimensional (upward from the ground to the pool);
- The ground is semi-infinite and the temperature at infinite depth is equivalent to the ambient temperature;
- There is perfect thermal contact between the ground and the cryogenic liquid, and the ground surface temperature equals to the liquid boiling point;
- The cryogenic liquid is at its boiling point and forms a thin pool of uniform temperature;
- The thermal properties of the ground are constant;

This model, called the one-dimensional (1D) conduction model, is relatively simple in terms of its mathematical formulation:

$$\frac{\partial T}{\partial t} = \alpha \frac{\partial^2 T}{\partial z^2} \qquad (1)$$

$$T = T_i \qquad at\ z \in \langle 0,\infty \rangle \qquad for\ t = 0$$

$$T = T_b \qquad at\ z = 0 \qquad for\ t > 0$$

$$T = T_i \qquad at\ z = \infty \qquad for\ t > 0$$

where,

T_i Initial temperature of the substrate and temperature at infinite depth, K

T_b Boiling temperature of the cryogenic liquid, K

t Time, s

α Thermal diffusivity of the substrate, $m^2\ s^{-1}$

z Distance measured downwards from the surface of the ground, m

The solution of the model for heat flux q_{cond} (in $W\ m^{-2}$) and temperature T at a given depth z in the ground is:

$$q_{cond} = k \frac{\partial T}{\partial z} = \frac{k}{(\pi \alpha)^{0.5}} (T_i - T_b) t^{-0.5} \exp\left(\frac{-z^2}{4\alpha t}\right) \qquad (2)$$

$$T = T_i - (T_i - T_b) erfc\left(\frac{z}{2\sqrt{\alpha t}}\right) \qquad (3)$$

where,

k Thermal conductivity of the substrate, $W\ m^{-1}\ K^{-1}$

Heat flux to the pool from the ground is given by:

$$q_{cond} = k\frac{\partial T}{\partial z}\Big|_{z=0} = \frac{k}{(\pi\alpha)^{0.5}}(T_i - T_b)t^{-0.5} \quad (4)$$

Briscoe and Shaw[10] suggested the insertion of an extra parameter, χ, in Equation 2 to take into account the fact that boiling rate tend to increase significantly with the surface roughness (as described in details in Section 2.2.5). However, there was no mention of how this parameter is calculated. They used a factor of 3 as the parameter to be able to fit the experimental data on vaporization rates of LNG spill produced by Burgess and Zabatekis [13] and American Gas Association [14]. Briscoe and Shaw [10] mentioned that the value of 3 can be used for other cryogenic liquid spills but this hypothesis should be confirmed with experimental data.

The 1D conduction model is currently very widely used in existing consequence modelling software packages. However this approach, while convenient for its simplicity, presents several limitations:

- The model inherently assumes that the heat flux to the pool is infinite at time zero, which is incorrect;
- The model does not take into account the possible limitation of the heat flux from the ground due to the formation of bubbles or a vapor film on the ground surface during the boiling, as described below. This assumption, while seen as conservative, tends to over predict the vaporization rate;
- The model assumes constant thermal properties of the substrate. Such properties are temperature dependent [10].

Due to the aforementioned limitations, it is necessary to use models that reduces the major limitation of perfect thermal contact. To be able to use such models it is

important to understand the physical phenomena of boiling, the underlying principles and criteria used in the models.

2.2 Pool boiling phenomena

When spilled onto a substrate at a temperature significantly higher than its boiling point, a liquid may undergo different consecutive boiling regimes, depending on the temperature difference between the liquid and the surface of substrate. This phenomenon was first experimentally highlighted in 1934 by Nukiyama [15] who immersed metal heating elements (platinum, nickel or nichrome metal wires or flat circular metal plates) of different dimension in water and measured the resulting heat flux from the heating element to the water (q in W/m^2) as a function of the wall superheat (ΔT in K, difference between surface temperature of the heating element, T_{surf}, and liquid temperature assumed to be the boiling point, T_b). Figure 2 shows the resulting $q = f(\Delta T)$ plot, called *boiling curve*. Nukiyama showed that the heat transfer coefficient is not a monotonic function.

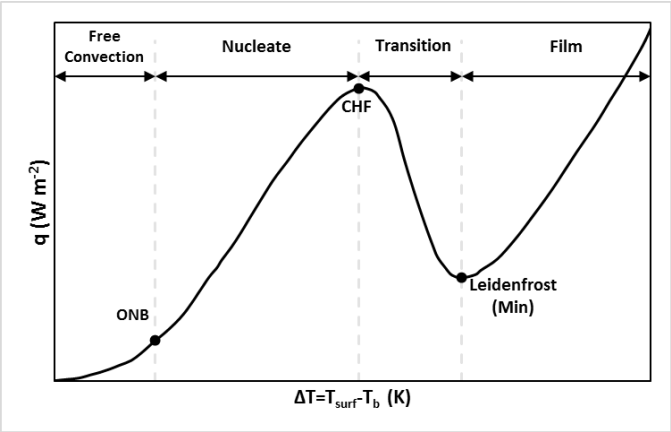

Figure 2: Boiling curve (Nukiyama, 1934) [15]

2.2.1 Film boiling

If ΔT is large enough, ***film boiling*** regime occurs. This regime is characterized by the formation of film of vapor at the surface of the substrate, making a clear separation between the liquid and the ground surface. This thin vapor film layer reduces the overall heat transfer from the surface to the liquid. The heat transfer in the vapor film is assumed to be laminar so that conduction is taken as the dominant heat transfer mechanism in the uniform layer of film [16]. Figure 3 shows a photograph obtained in the photographic study of film boiling of liquid nitrogen (LN_2) with a noticeable stretch of vapor film just above the substrate [17].

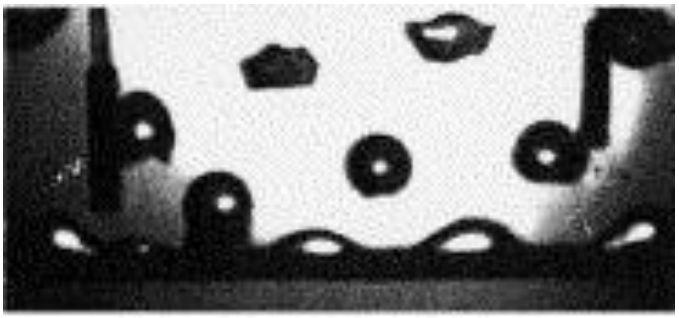

Figure 3: Photograph of film boiling regime of liquid nitrogen [17]

The thermal conductivity of a vapor film being much less when compared to that of a liquid [16], the overall heat transfer coefficient from the substrate surface to the liquid is greatly reduced. This heat transfer coefficient in the film boiling regime decreases as the vapor film grows in size.

The heat transfer rate in film boiling regime decreases with ΔT (Figure 2). This happens when the grounds cools since there is continuous transfer of heat from the ground to the pool. At a certain point, the ΔT reaches a minimum below which the heat transfer from the ground is not enough to sustain the vapor film. The value of ΔT at this particular point is called the *Leidenfrost point* (Figure 2), named after Gustav Leidenfrost, who studied the phenomenon of continuous existence of liquid droplet when it is in contact with a hot surface until the heat causes the droplet to evaporate. This phenomenon explains the eventual evaporation of water droplets when in contact with a hot plate. The same phenomenon occurs with liquid nitrogen when dropped on room temperature floor. The liquid nitrogen persists for few seconds before disappearing [18]. The Leidenfrost point corresponds to the minimum heat flux in boiling regime.

2.2.2 Nucleate boiling

As the ground cools down (decreasing ΔT), the vapor film characteristic of the boiling regime breaks, and the contact between the liquid and the surface is enhanced. This regime is called *nucleate boiling regime* and is characterized by bubble formation at the nucleation sites of the solid surface, vapor bubble growth and bubble departure from the solid substrate making the heat transfer from the solid substrate to the liquid more efficient [11,16]. The heat transfer rate in nucleate boiling regime also decreases with ΔT (Figure 2). The heat flux in nucleate boiling regime reaches a minimum value when ΔT reaches the Onset to Nucleate Boiling (ONB) point (Figure 2). For ΔT values lower than the ONB heat transfer by free convection occurs. The heat flux in nucleate boiling regime reaches a maximum value when ΔT is at the Critical Heat Flux (CHF) or the maximum nucleate boiling (burnout) heat flux.

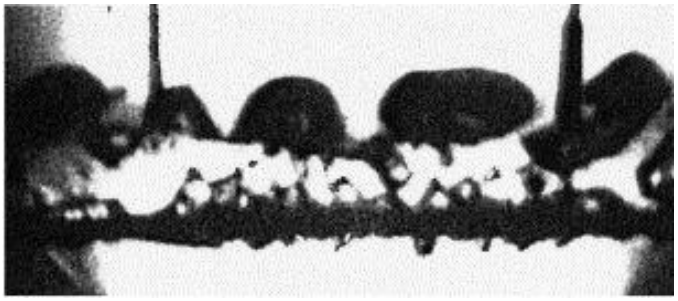

Figure 4: Photograph of nucleate boiling regime of liquid nitrogen [17]

Figure 4 shows the bubble formation, growth and departure from the surface of the solid substrate obtained in the study of nucleate boiling of liquid nitrogen [17]. It has been

noted in literature that bubbles appear randomly on the surface in this regime. In the late 1950s, it was shown theoretically [19] that cavities, pits and rough patches on the surface of the solid substrate are the plausible nucleating sites for bubble formation, where vapor embryo (bubble of vapor at the earliest stage of its formation) are formed. This was later validated experimentally by Clark *et al.*[20]. The nucleation site density (number of active nucleation site per surface area) plays a key role on the boiling rate. This density tend to increase with ΔT and is a function of the attributes of the surface of the solid substrate (e.g. surface finish, surface wettability, thermal properties and the thickness of the substrate) [21].

Once the bubble is formed, it grows in a saturated liquid until it reaches a critical size, separates from the solid surface and rises up through the liquid pool [21,22].

Two approaches were developed to predict the ONB point of a liquid:

- One approach states that the ONB is reached when a vapor embryo (bubble of vapor at the earliest stage of its formation) at the surface of the solid substrate is surrounded by superheated liquid at all vapor-liquid interface [23].
- The other approach states that the ONB corresponds to the ΔT at which the vapor-liquid interface becomes stable (stability being reached when an increase in volume of the bubble increases the curvature of the vapor/liquid interface [23], without breaking the bubble.

The CHF is determined by applying Helmholtz instability criterion which defines the maximum heat flux at which the vapor generation is stable and leads to maximum mixing of liquid and vapor bubbles at the solid surface [24].

2.2.3 Transition boiling

The transition between film boiling and nucleate boiling regimes (ΔT between CHF and Leidenfrost point, see Figure 2) is called *transition boiling regime* [16]. Both the vapor film formation and bubble formation at nucleation sites coexist in the transition regime, which implies that each point on the boiling surface has alternate contact with liquid and vapor [25] as experimentally demonstrated by Berenson [24]. Figure 5 shows a photograph obtained in the study of transition boiling of liquid nitrogen [17].

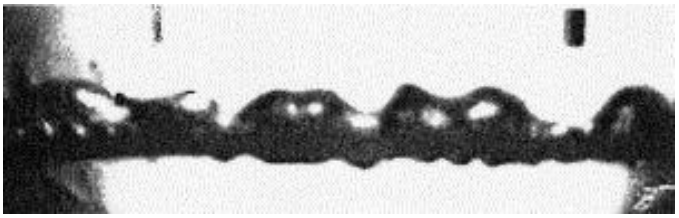

Figure 5: Photograph of transition boiling regime of liquid nitrogen [17]

Transition boiling has been the least explored regime among all the three regimes of boiling [21], which is probably due to the difficulty in conducting experiments in this region.

2.2.4 Modeling of boiling regimes

There are few theoretical correlations that have been developed to calculate the heat flux to the pool for the three boiling regimes. These were summarized by Kalinin *et*

al. [25]. They proposed the following equation for transition boiling heat flux, q_t. It is important to note that the solid substrate is referred to as wall in the following correlations.

$$q_t = q_n f + q_f(1 - f) \quad (5)$$

$$f = (1 - \Delta T^*)^7 \quad (6)$$

$$\Delta T^* = \frac{\Delta T_w - \Delta T_{Cr}}{\Delta T_{min} - \Delta T_{Cr}} \quad (7)$$

where,

f	Averaged fraction of the surface in contact with liquid at a given time.
q_n	Nucleate boiling heat flux, W m^{-2}
q_f	Film boiling heat flux, W m^{-2}
ΔT^*	Dimensionless temperature difference
ΔT_w	Temperature difference, T_w-T_s, K
T_w	Temperature of the wall, K
T_s	Saturation temperature of the liquid, K
ΔT_{Cr}	Temperature difference at the Critical Heat Flux point, K
ΔT_{min}	Temperature difference at the Leidenfrost point, K

The expression for *f* was an approximate equation developed by Kalinin *et al.* by using the experimental data from six literature sources [25].

Kalinin *et al.* suggested the following empirical expression, Equation 8, for nucleate boiling heat flux, q_n, which was developed by Grigoryev *et al.*[26], to be used in Equation 5. This empirical expression takes into account the unsteady thermal conductivity associated with the growth and departure of vapor bubbles from the heated

surface during nucleate boiling. Incorporating the unsteady thermal conductivity into the boiling regimes model improves its representation of nucleate boiling significantly.

$$q_n = \frac{4.1[1 + 10\left(\frac{\rho_{vs}}{\rho_l - \rho_{vs}}\right)^{\frac{2}{3}}]^3 \Delta T_w^3}{\sigma T_s \left(\frac{\sqrt{\nu_l}}{k_l} + \frac{10}{\sqrt{\rho_w C_{pw} k_w}}\right)^2 \left(1 + 10\sqrt{\frac{\rho_l C_{pl} k_l}{\rho_w C_{pw} k_w}}\right)} \quad 8$$

where,

ρ_{vs} Density of the saturated vapor, kg m^{-3}

ρ_l Density of the liquid, kg m^{-3}

ρ_w Density of the wall, kg m^{-3}

ν_l Kinematic viscosity of the liquid, m^2 s^{-1}

k_w Thermal conductivity of the wall, W m^{-1} K^{-1}

k_l Thermal conductivity of the liquid, W m^{-1} K^{-1}

C_{pl} Specific heat capacity of the liquid, J K^{-1}

C_{pw} Specific heat capacity of the wall, J K^{-1}

The following expression for film boiling heat flux, q_f, was developed by Kalinin *et al.* [27].

$$q_f = 0.18 k_{vf} \Delta T_w \left[\frac{g}{\nu_{vf} \alpha_{vf}} \left(\frac{\rho_l}{\rho_{vf}} - 1\right)\right]^{\frac{1}{3}} \quad 9$$

where,

k_{vf} Thermal conductivity of the vapor film, W m^{-1} K^{-1}

α_{vf} Thermal diffusivity of the vapor film, m^2 s^{-1}

g Gravitational acceleration, m s^{-2}

ρ_{vf} Density of the vapor film, kg m^{-3}

The temperature difference at the Leidenfrost point, which is used in Equation 7, is given by the following correlation developed by Kalinin et al [28]. Using this expression will result in an error of at most ± 20% [25].

$$\Delta T_{min} = (T_c - T_l)\left[0.16 + 2.4\left(\frac{\rho_l C_{pl} k_l}{\rho_w C_{pw} k_w}\right)^{\frac{1}{4}}\right] \quad 10$$

where,

T_c Temperature at critical point, K

T_l Temperature of the liquid, K

The temperature difference at the critical heat flux is determined by equating Equation 8 and Kutateladze correlation (Equation 12) for maximum heat flux [29,30]. The final expression for ΔT_{Cr} is given in Equation 11 [30].

$$\Delta T_{Cr} = 0.625(q_{Cr}\sigma T_s)^{\frac{1}{3}} \frac{\left(\frac{\sqrt{\nu_l}}{k_l} + \frac{10}{\sqrt{\rho_w C_{pw} k_w}}\right)^{\frac{2}{3}}\left(1 + 10\sqrt{\frac{\rho_l C_{pl} k_l}{\rho_w C_{pw} k_w}}\right)^{\frac{1}{3}}}{1 + 10\left(\frac{\rho_{vs}}{\rho_l - \rho_{vs}}\right)^{\frac{2}{3}}} \quad 11$$

$$q_{Cr} = 0.16\lambda\rho_{vs}^{\frac{1}{2}}[\sigma g(\rho_l - \rho_{vs})]^{\frac{1}{4}} \quad 12$$

where,

q_{Cr} Critical heat flux, W m^{-2}

σ Surface tension, N m^{-1}

λ Latent heat of vaporization, J g^{-1}

The boiling regimes model assumes that Equation 8 and Equation 9 can be linearly extrapolated through the transition regime [25].

It is important to note that these correlations were developed from experiments conducted using non-cryogenic liquid on metal surfaces. However, in order to use these correlations model for cryogenic liquid spill, they need to be validated against experimental data obtained from cryogenic liquid spill on solid substrates.

2.2.5 Effect of surface roughness on boiling

In 1960, Kurihara and Myers [31] showed that surface conditions, especially roughness of the substrate, have a significant effect on the boiling curve as the number of active nucleation sites increases with roughness.

In 1962, Berenson [24] published the study of the boiling rate of pentane and carbon tetrachloride on different surfaces like copper, Inconel and nickel with different surface conditions. Figure 6 and Figure 7 respectively show the results he obtained for the boiling of pentane on copper and Inconel surfaces of the following increasing level of roughness[†]: *mirror finish* (smoothest), *emery 320*, *emery 60* and *lapped finish* (roughest). It can be observed that, in the film boiling regime, the heat flux is independent of the surface roughness (the peak roughness height of the solid surface being less than the vapor film thickness). Other experiments also demonstrated that the surface cleanness and the surface material do not affect the film boiling regime. Very importantly Berenson demonstrated

[†] Here roughness level describe the nucleation site density.

that the transition and nucleate boiling regimes are highly sensitive to the surface roughness. As shown in Figure 6 and Figure 7 there is a shift of the nucleate boiling regime to the left of the boiling curve as the surface roughness increases. Indeed, the heat transfer rate in nucleate boiling regime can increase by a 500-600% depending on the surface roughness. In other words, for a given ΔT, the nucleate boiling heat flux is higher in the case of a rougher surface. Berenson observed that CHF is independent of surface roughness as the difference is within 10 %, which is generally the within the error limit in engineering considerations.

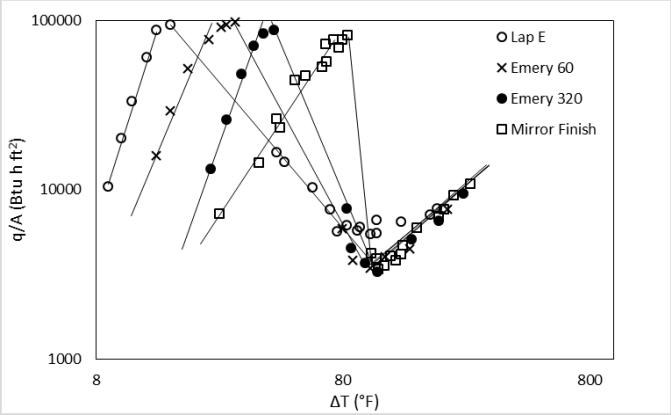

Figure 6: Effect of surface roughness on the boiling curve of pentane on copper [24]

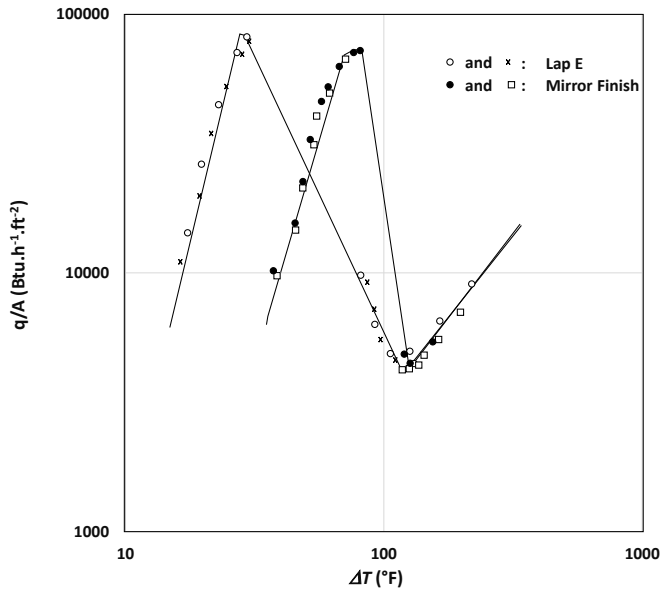

Figure 7: Effect of surface roughness on the boiling curve of pentane on Inconel [24]

In 1985, Bui and Dhir [32] studied the behavior of transition boiling heat transfer by conducting experiments with saturated water on isothermal vertical surface. Figure 8 shows the boiling curve that was obtained in this experiment for smooth mirror finish and rough emery grade 600 finish surface. The authors showed that as the surface roughness increases the left part of the boiling curve tends to shift to the left (close to nucleate boiling region). However , contrary to Berenson [24], they observed that the CHF (maximum heat flux) increases and tends to occur at lower ΔT for rougher surfaces.

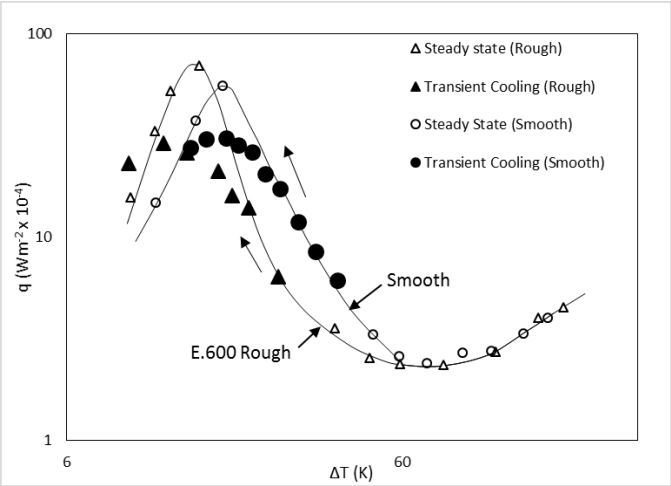

Figure 8: Effect of surface roughness on the boiling curve of water [32]

2.2.6 Effect of chemical composition on boiling

It is common practice to assess the LNG source term by using the properties of pure methane (on the basis that methane is the main constituent of LNG) or by using the properties of a pseudo-component of constant composition. This approach is questionable as the vaporization rate of a mixture may differ from that of a pure component due to preferential boiling of lighter components [33]. The difference in pure and binary systems boiling can be explained using the phase equilibrium diagram of a binary system. In this diagram, the mole fraction of one of the components is plotted on the abscissa and the boiling temperature of the mixture on the ordinate. One such example of vapor liquid equilibrium (VLE) phase envelope is of methane-ethane binary system. Conrado and Vesovic[34] studied the binary system consisting of 90 % methane and 10 % ethane and the VLE phase diagram is shown in Figure 9. As seen in the diagram, the dew point curve is

very steep for pure methane and the bubble point curve is flat. This implies that during the initial stages of the spill, the vapor generated will mostly consist of methane and the liquid boiling temperature will change very slowly as shown by the flat bubble point curve. This is because methane is the lighter component with lower latent heat of vaporization than ethane and hence a lower boiling point. Similarly, the VLE phase diagram shows that during the later stages of the spill, there is not much change in vapor composition but the boiling temperature of the liquid increases rapidly which is shown by the bubble point curve towards the pure ethane end. The dew point curve becomes flatter towards the ethane end of the VLE phase diagram [34].

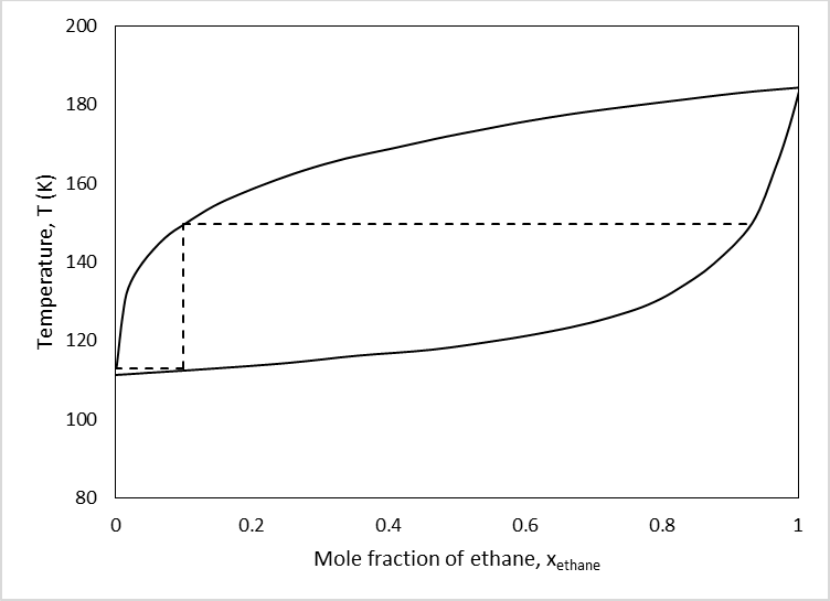

Figure 9: Phase equilibrium diagram of methane-ethane binary system [34]

Conrado and Vesovic also simulated the graph illustrated in Figure 10 that shows the boiling temperature of the LNG liquid pool over time affected by vaporization. It also

shows the mole fraction of methane in the liquid phase on the secondary axis as the pool vaporizes with time [34]. Figure 10 shows how the boiling point of LNG mixture remains the same with changes in mole fraction of methane in the remaining liquid for the first 80 s. It also shows during the later stage, with small change in liquid composition of methane, the boiling point of the liquid has a sharp increase. Therefore, Figure 10 is well explained by VLE phase diagram that is illustrated in Figure 9.

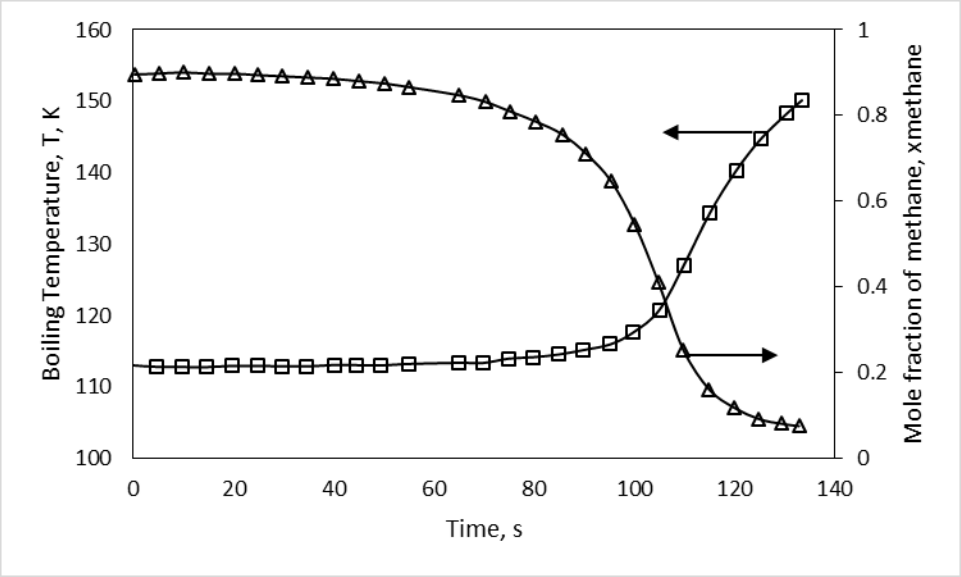

Figure 10: Boiling temperature of LNG and mole fraction of methane in the liquid phase with time [34]

The effect of the liquid composition on pool boiling was investigated by Collier and Thome [35] in 1994 when they presented the primary changes in the pool boiling curve of binary mixture versus a pure liquid in a schematic diagram (Figure 11). They pointed out that the onset of nucleate boiling of a binary mixture occurs at a higher ΔT than a pure liquid. This is due to the temperature gradient that exists in the pool due to the variable

liquid composition. The heat transfer coefficient of the nucleate boiling regime decreases considerably for a binary mixture. The CHF either increases or decreases depending on the convection effects associated with mixing of vapor and liquid in the pool. The Leidenfrost point increases and is shifted towards higher ΔT for a binary mixture. There is also an increase in the heat transfer rates of the film boiling regime for a binary mixture [35].

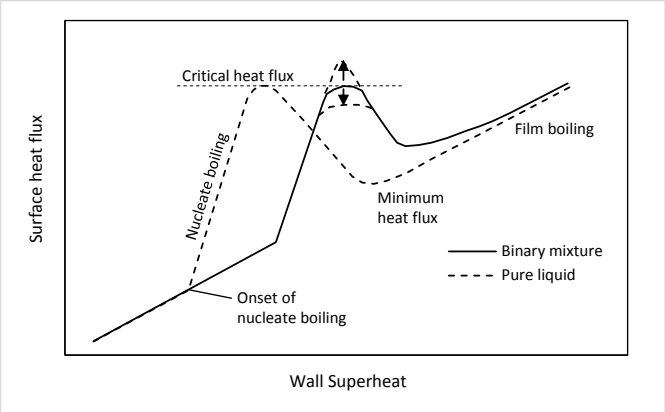

Figure 11: Schematic diagram depicting the principle changes to pool boiling curve for binary mixture [35]

The schematic diagram in Figure 11 was developed based on experiments done using non-cryogenic binary liquids. In 1961, Sternling and Tichacek [36] conducted experiments using fourteen binary systems (prepared using water, light alcohols and heavy oils) to observe the nucleate boiling of binary liquids. They observed that the heat transfer coefficient was lower for binary mixtures than for pure components (with the same physical properties) at a given heat flux. Lowery and Westwater (1957) [37] and Van Stralen [38] (1959) studied the addition of methanol and water, respectively, to single components

and observed an increase in CHF for binary mixtures when compared to pure components. In the case of transition boiling regime, only one report developed by Happel and Stephan [39] in 1974 showed qualitatively that binary mixture influence on transition boiling regime is the same as that in nucleate. They conducted pool boiling experiments with benzene-toluene, ethanol-benzene and water-isobutanol. Van Stralen *et al.* [40] in 1972 studied the film boiling of water-2-butanone mixture on a thin wire and observed that the binary mixture produced vapors by utilizing 53% of the heat from the surface whereas, pure components utilized 95%. As a result they concluded that the Leidenfrost point for binary heat flux will be higher than that of a pure liquid [40]. Since lesser fraction of heat from the surface was used by the binary mixture in the production of vapor film, more heat transfer will be required to sustain the vapor. Therefore, as the heat transfer decreases with decreasing ΔT, the breaking of film for binary mixtures will occur at a higher ΔT. For the prediction of film boiling regime, the experimental study of Yue and Weber [41] (1973) was used. They studied the film boiling regime of binary mixtures on a vertical plate.

In 2012, Fernandez *et al.* [42] published an integral model for pool spreading, vaporization and dissolution of multicomponent pool. This model is robust and was applied for boiling and evaporation. The model takes into account the preferential boiling of LNG and has been validated using the experiments conducted by Burgess *et al* [13]. In 2014, Basha *et al.* [33] developed a model that includes the VLE calculations. This model was validated using experiments conducted by Moorhouse and Carpenter [11].

2.3 Experimental study of the boiling of cryogenic liquid in the published literature

All the observations summarized for the boiling behavior of liquids on solid substrates, described above, have been performed using non-cryogenic liquids. However, the focus of this work is on cryogenic liquid spill on solid substrates. Therefore, a comprehensive literature survey is performed on the existing experimental study of cryogenic liquid boiling and is summarized in Table 1.

Table 1: Previous notable experimental work on cryogenic liquid boiling

Author, Year	Cryogen	Substrate	Results	Comments
Reid and Drake [43], 1975 Reid and Wang [44], 1978 Reid [45], 1980	Liquid nitrogen Liquid methane LNG	Soil Sand Concrete (Four types) Polyurethane Corrugated aluminum	LNG had higher boiling rate than liquid nitrogen or liquid methane. This could be due to foaming in LNG. Enhanced boiling rates was observed due to percolation into the soil or sand. Plastic barrier between pool and test substrate reduced boiling rates. Vaporization of LNG evolved pure methane until its concentration in the residual liquid dropped below 20%. One type of insulating concrete and corrugated aluminum were termed promising materials fdike floor as the substrates produced low boiling rates.	Experimental results agreed with the simple 1D model predictions. Possibility of film boiling mentioned but not observed. The boil off rates on all the other substrates had deviation when identical experiments were conducted.

Table 1: Continued

Author, Year	Cryogen	Substrate	Results	Comments
Moorhouse and Carpenter [11], 1986	LNG	Steel Soil Concrete (ordinary and lightweight) Limestone chippings	For concrete, the boil off rate does not exceed 0.5 kg m^{-2}. In the case of particulate materials, the boil off rates are higher due to the contribution from the total surface area of the particles. Water content increases the decline in boil off rates. Materials that have low density, low water content and are impervious should be used as dikes.	Boil off rates matched simple theoretical predictions
Takeno et al. [46], 1994	Liquid hydrogen Liquid oxygen	Concrete Sand	Ice formation in the sand and penetration in the sand and concrete were different for liquid hydrogen and oxygen. These phenomena depends on density. Viscosity, surface tension and latent heat of vaporization.	The experimental results were in good agreement with the simple 1D model but the ice formation and liquid penetration were not quantified. Therefore, it lacks credibility. May allow for preliminary assessment of models.

2.4 Bridging the gaps in the literature

There are excellent works on cryogenic boiling published in the literature to date. These experimental data have been used to model the behavior of boiling of cryogenic liquid on solid substrate. However, these experimental studies have used 1D conduction model that does not take into account the physics of film boiling thereby not representing the actual boiling process. Therefore, this approach can be questioned. The correlations developed in the literature to represent each boiling regime were based on experiments conducted using non-cryogenic liquids. Therefore, its validity on the boiling of cryogenic liquids can also be questioned. As a result, this work compares the boiling regimes model prediction to the experimental data.

The study of boiling on rough and smooth surfaces were done only for non-cryogenic liquids. However, the surface roughness was not characterized in the said studies. There is no literature available for effect of surface roughness on cryogenic liquid boiling. Therefore, this effect will be explored in this research and compared to the existing experimental data on non-cryogenic boiling. An attempt will be made to characterize the surface roughness. In the case of modelling, there is no correlation found in the literature that accounts for surface roughness in a quantifiable manner.

The schematic diagram that was developed for pure vs. binary mixture boiling rates were based on non-cryogenic experimental data. As a result, similar behavior needs to be studied for cryogenic liquid so as to improve the models to account for binary

mixture effect. This work provides experimental results for the development of such models.

There have been experiments performed with cryogenic mixtures such as LNG and the need for studying composition effects was highlighted. However, no study have done experimental study of pure and binary mixture on solid substrate to be able to accurately model the effect of composition on the resulting boiling rates. Therefore, this work conducts experiments using pure (liquid nitrogen) and binary (liquid nitrogen/oxygen mixture) mixtures on concrete (typical dike floor material) and makes the experimental data available for future model development to account for preferential boiling in mixture.

The experiments available in the literature are not well instrumented for future model validation. Also, these experiments did not generate the boiling curve and hence, failed to clearly identify the boiling regimes. The CHF and Leidenfrost point were not determined. Therefore, this work aims at clearly distinguish the boiling regimes that are observed on the solid substrate and determine the CHF and Leidenfrost points, wherever possible.

3. SCOPE OF WORK

The objective of this research is to make an attempt in bridging the gaps identified in the existing literature on LNG boiling. To implement this objective, a series of experiments will be conducted by spill of cryogenic liquids on solid substrates to study the contribution of conductive heat flux and the experimental data will be made available for development of models in the future. The boiling regimes (film, transition and nucleate) will be clearly identified in each experiment for clear distinction between them. The experiments will be performed using liquid nitrogen and liquid nitrogen/oxygen mixture as a safer analogue to liquid methane and LNG.

To capture the behavior of cryogenic boiling (liquid nitrogen) on different substrates, a wide range of solid substrates are chosen based on thermal conductivity with concrete having low thermal conductivity and steel having relatively high thermal conductivity. Polystyrene, being a heat insulator, is chosen to study the transition from boiling to evaporation by limiting conduction effects from the substrate.

The effect of surface roughness will be captured using two types of concrete substrate (smooth and rough). The surface roughness will be quantified and the boiling behavior of liquid nitrogen will be clearly represented. This will help in using the experiments to develop models that account for surface roughness since this parameter has been identified to significantly affect boiling rates of liquids.

To study the effect of pool composition on its boiling rate, liquid nitrogen (pure) and liquid nitrogen/oxygen mixture (binary) will be spilled on smooth surface concrete.

The specific liquid combination is chosen because of the correlation between LNG and liquid nitrogen/oxygen mixture. The most dominant component of LNG and liquid nitrogen/oxygen mixture is methane and nitrogen, respectively. If LNG is considered a binary mixture of methane/ethane in the 80:20 ratio and compared to liquid nitrogen/oxygen mixture in the same ratio, it could be seen that the major component (methane, nitrogen) in each mixture has the lower boiling point than the minor components (ethane, oxygen). Therefore, use of liquid nitrogen and liquid nitrogen/oxygen mixture in the experiments of this work will provide a similar picture if liquid methane and LNG were to be studied. As a result, this work could be used to improve models and account for mixture composition through VLE calculations.

The experimental setup will be designed for the direct measurement of the vaporization rate of the cryogens on the different substrates. For this measurement, the setup will be heavily instrumented to measure temperature and heat flux at different locations inside the substrate. The temperature of the pool will also be measured in order to determine if the pool is in the boiling regime (pool at boiling point) or in the evaporation regime (pool at a temperature below the boiling point).

The generated experimental data will be analyzed to determine the vaporization rate and generate the experimental vaporization rate vs. time curve. The comparison of concrete data with the prediction of the 1-D conduction model and the boiling regimes model will be performed. For modeling, the temperature-dependent thermal properties of concrete will be used. The differences observed will be discussed and recommendations for the use of existing source term models will be done.

Although, this research study focuses on laboratory scale experiments, there will be medium and large scale experiments performed on the same type of substrate (specifically concrete with the same composition) as a continuation to this research study. This is done to have consistency in the data obtained when experiments are extended to field scale.

4. METHODOLOGY

As mentioned in literature review, the knowledge gaps include lack of experimental data on cryogens spilled on concrete, especially large scale, which could be used to validate the mathematical models of the vaporization rate, which include, the effect of solid substrate the effect of surface roughness and liquid. This has been addressed in this work by experimental approach and the result of the experiments has been compared to some of the existing models. Previously described scope of work and the methodology of this work is graphically described in Figure 12. To study the effect of type of substrate on the boiling of cryogens, liquid nitrogen is spilled on substrates having a wide range of thermal conductivities: concrete (low) and steel (high). The effect of surface roughness is studied through boiling of liquid nitrogen on smooth and rough surface of concrete. The composition effect is studied through boiling of liquid nitrogen and liquid nitrogen/oxygen mixture on concrete.

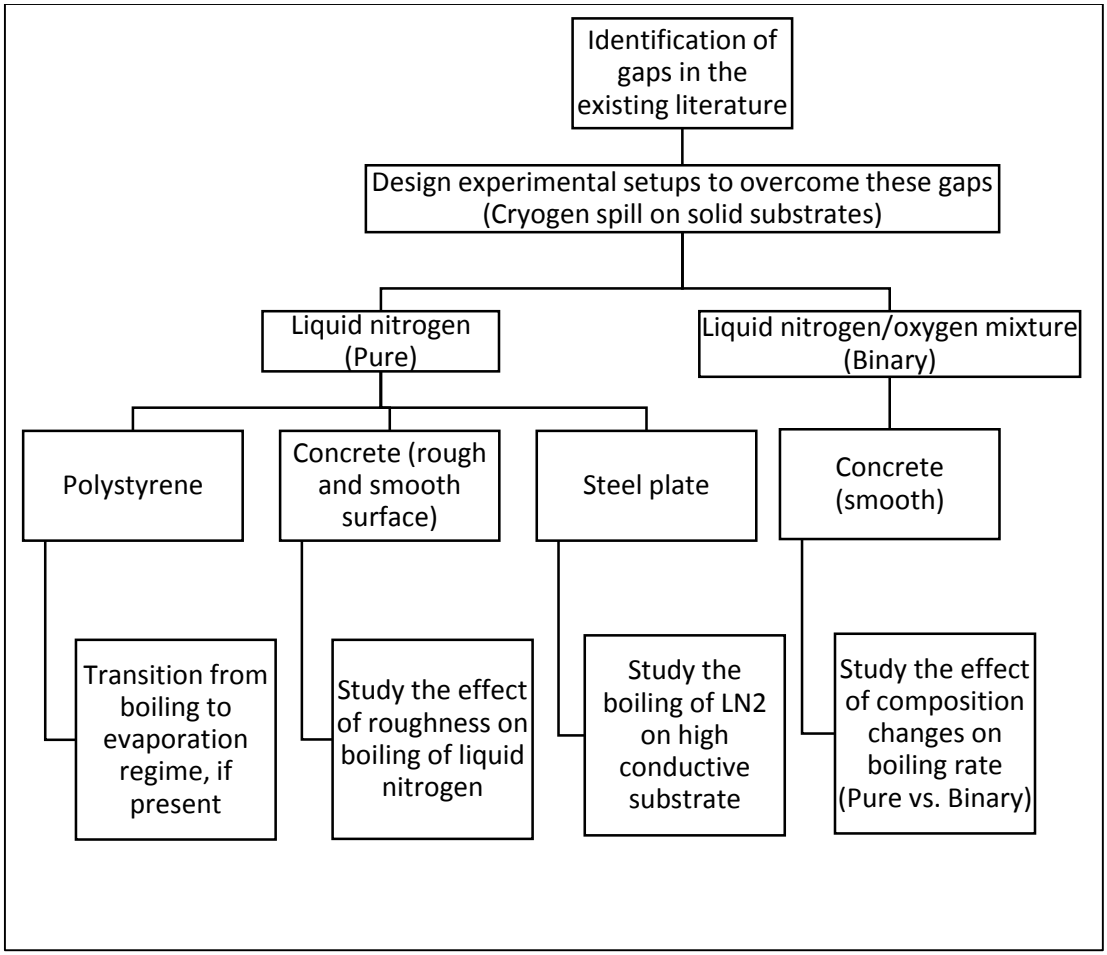

Figure 12: Schematic of methodology

A series of laboratory scale experiments were designed and instrumented to perform the spill of cryogenic liquid (liquid nitrogen and liquid nitrogen/oxygen mixture) on different substrates (concrete, steel) (Figure 13). The overall vaporization rate of the liquid has been measured through mass monitoring and has been used to estimate the overall heat flux provided to the pool assuming the boiling regime of the pool, which means its constant temperature at boiling point. This temperature was monitored by thermocouples installed in the pool. The heat flux to the pool was measured at the wall

and the base at particular depths. The wall heat flux was used to estimate the heat flux provided through the walls and thus subtracted from the total heat flux to the pool, which gave the conductive heat flux. The convective heat flux was neglected.

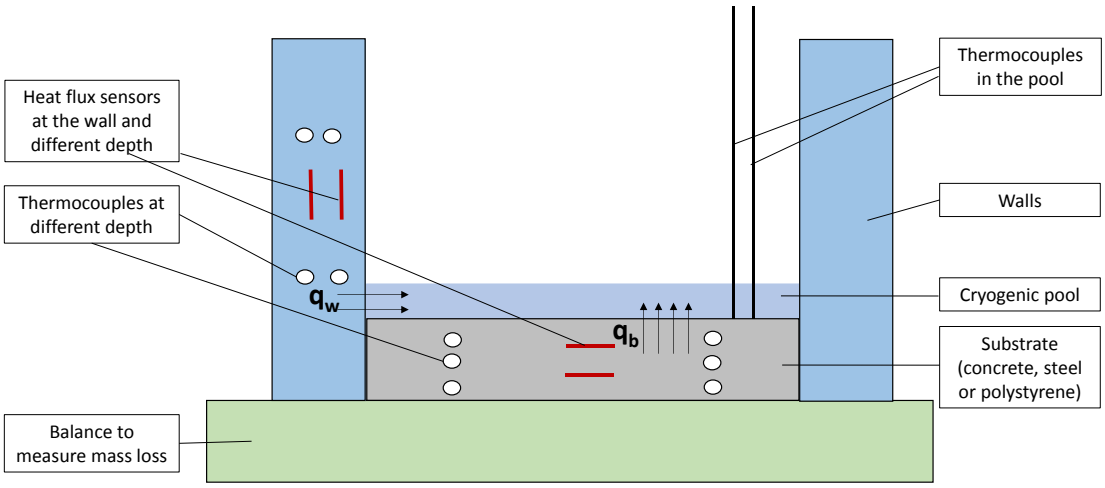

Figure 13: Schematic of general experimental setup

After the design of the experimental setups, each experiment was performed by spilling cryogenic liquid into the container. The liquid was refilled several times, each time before the box was empty. The refilling of the box is demonstrated by mass increase in Figure 14. A typical fill/refill lasts about 3-4 s.

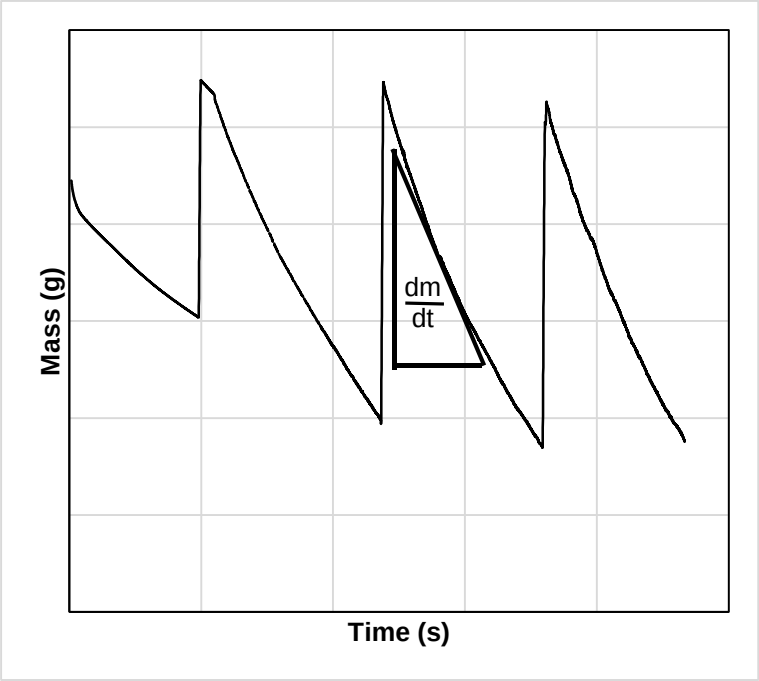

Figure 14: A typical mass measurement during the experiment

4.1 Determination of vaporization rate and conductive heat flux

Each experiment yields a mass *m* as function of time as shown in Figure 14 and the first derivative of this mass loss (excluding refilling) is the overall vaporization rate, V_{wb} (Equation 13). This was obtained by calculation of the change in mass over the 1 second time *t* interval.

$$Vap.Rate\ (V_{wb}) = \frac{dm}{dt} = -\frac{m_{t+1} - m_t}{(t+1) - t} \qquad 13$$

The vaporization provided to the pool through the walls V_w was estimated based on heat flux measured inside the walls, q_w, as follow

$$V_w = \frac{q_w h_l l}{\lambda} \quad (14)$$

where λ is the latent heat of vaporization of the cryogen, l is the side length of the substrate and h_l is the height of liquid pool at a certain time. The height of the liquid h_l was calculated from the mass of liquid at that particular time using Equation 15.

$$h_l = \frac{m}{\rho_l A} \quad (15)$$

where A is the surface area (equal to l^2) of the substrate that is in contact with the liquid pool and ρ_l is the density of the cryogen.

Subsequently, the vaporization provided to the pool through the base V_b was calculated using Equation 16.

$$V_b = V_{wb} - V_w \quad (16)$$

and the heat flux to the pool due to conduction from the base q_b, using Equation 17.

$$q_b = \frac{\lambda}{A} V_b \quad (17)$$

4.2 Comparison with models

The experimental results are used to validate the prediction of 1D conduction model and so called boiling regimes one. The validation was done using the MATLAB code formulated by Quraishy [47], member of Mary Kay O'Connor Process Safety Center, research group at Texas A&M University at Qatar. Quraishy [47] studied a combination of liquid-solid system by utilizing methane, hydrogen, oxygen and nitrogen on the solid

substrates: concrete, steel, copper, aluminum and polystyrene. He has formulated boiling regimes model based on Kalinin *et al.* [27], Grigoryev *et al.*[26] and Kutateladze [29] correlations as explained in Section 2.2.4.

4.2.1 Thermal properties of solid substrate

Both of above mentioned models need thermal properties of substrate in order to estimate the vaporization rate. These thermal properties include thermal conductivity k and thermal diffusivity α, which can be calculated from k and the specific heat capacity C_p. These thermal properties are functions of the solid temperature, which change with time upon the spill. However, both models assume these properties as constants. Thus, in this work, in order to check how the change in these properties would affect an estimated vaporization, two separate calculations has been made for both models. First, the vaporization is evaluated with thermal properties of the substrate calculated at initial temperature of solid T_i, which represents the temperature at infinite depth in the solid, and second, it is evaluated at boiling point of the liquid T_b. In the case of concrete, the thermal properties at the two temperatures are determined using the data obtained from NETZSCH for thermal conductivity and specific heat capacity. The thermal diffusivity α is calculated using thermal conductivity k, specific heat C_p and density, ρ as per Equation 18. As a result, there are two values for each thermal property (thermal conductivity, thermal diffusivity and specific heat capacity); one at T_i and the other at T_b, these are summarized in Table 2

$$\alpha = \frac{k}{\rho C_p} \qquad 18$$

Table 2: Thermal properties of concrete at T_i and T_b

Temperature (K)	Thermal conductivity, k (W $m^{-1}K^{-1}$)	Specific heat capacity, C_p (J $kg^{-1}K^{-1}$)	Thermal Diffusivity, α (m^2s^{-1})
Ti=297	1.132	915.51	5.30 x 10^{-07}
Tb=77	0.617	259.90	1.02 x 10^{-06}

4.2.2 1D semi-infinite solid, "ideal" conduction model

The analytical solution to the 1D conduction model, which assumes semi-infinite solid and ideal contact of the liquid with the solid and thus constant temperature of the solid's surface equal to boiling point of liquid (Equation 2) was used to model the heat transfer from the substrate to the cryogen. The initial temperature of the substrate used in the model is measured during the experiment (ambient temperature). This model was evaluated using thermal properties of the substrate (solid) at two temperatures, T_i and T_b, as described in Section 4.2. A typical curve generated using 1D conduction model for heat flux provided to the pool q as a function of time is shown in Figure 15.

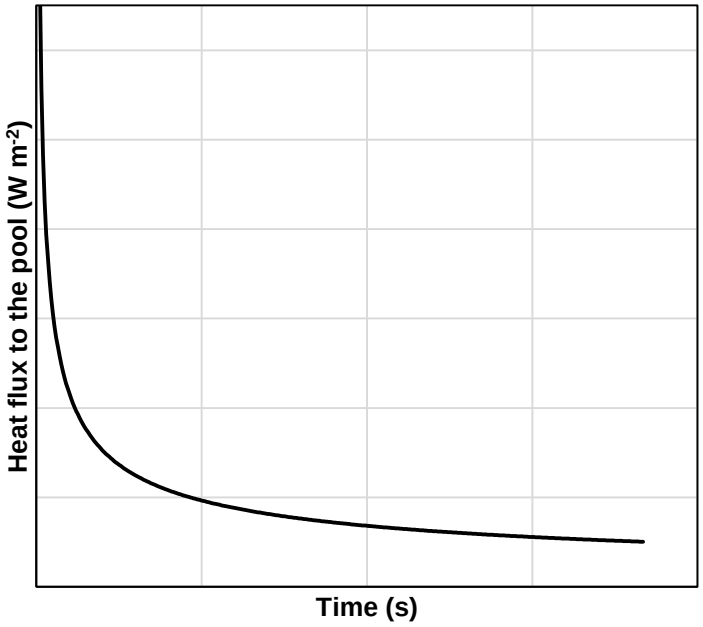

Figure 15: A typical curve obtained for heat flux provided to the pool as a function of time using 1D conduction model

The model was evaluated with the factor χ which is the roughness parameter as described in Section 2.1. The model was evaluated at two values of χ: 1 and 3. The value of 1 implied that no surface roughness was taken into account. The value of 3 was suggested by Briscoe and Shaw [10] to fit the model to the experimental data. As a result, this value was used here to check if the statement holds true.

4.2.3 Boiling regimes model

The boiling regimes model is a combination of all equations that describe the three regimes: film, transition and nucleate. As explained before, this model was formulated by

Quraishy [47] using the equations provided in Section 2.2.4. These equations can be used to generate the boiling curve, which is the heat flux provided to the pool q as a function of temperature difference between the liquid boiling point and solid surface ΔT (Figure 2). The model was evaluated using thermal properties of the substrate (solid) at two temperatures, T_i and T_b, as described in Section 0. A typical heat flux provided to the pool q as a function of time t determined by this model is shown in Figure 16.

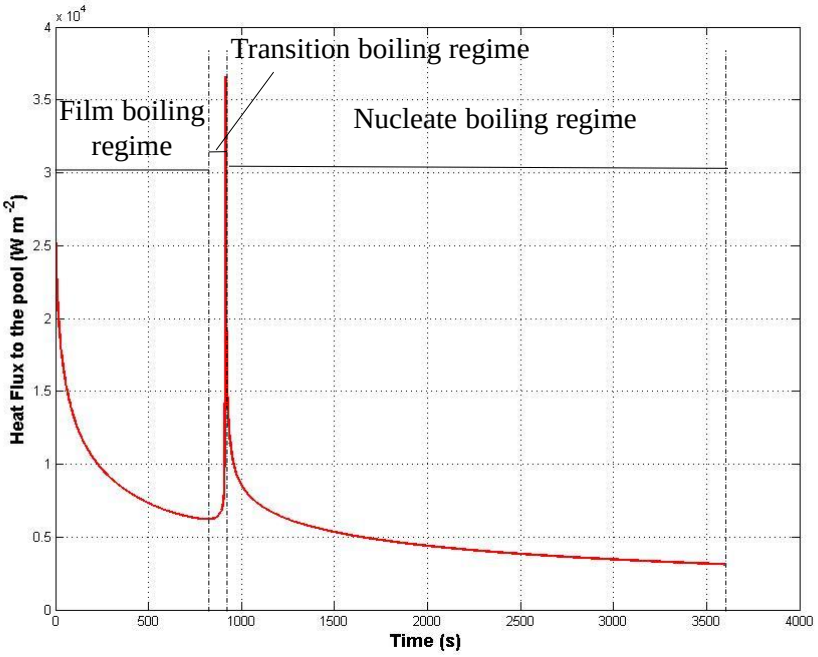

Figure 16: Heat flux to the pool vs. time curve generated from the boiling curve

5. EXPERIMENTAL SETUP

Four experimental setups have been prepared which include the container of different base: rough and smooth surface concrete, steel and polystyrene. The overall vaporization rate of the liquid has been monitored by Mettler-Toledo balance. The heat flux sensors and thermocouples (by OMEGA) instrumented in the setup were connected to the Data Acquisition system (DAQ) built using IOtech components. The balance was connected through National Instruments converter and data recorded through LabView. Both data logs were synchronized. The details of sensors are provided in detail in Section 0. Comprehensive risk assessment was carried out before conducting experiments (provided in Section 0) and checklist was prepared to keep track of all the necessary steps before the experiments (Section 0).

5.1 Concrete base

Both rough and smooth surface concrete base setups were designed in an identical manner as shown in Figure 17. Each of them consists of two concrete slabs of dimension 300 mm x 300 mm x 50 mm placed on top of each other. The top slab had top surface either smooth or rough. For the smooth setup, the top surface, the surface that will be in contact with cryogen, was obtained by polishing. The rough concrete surface was obtained during a standard concrete pouring as it is used at most of industrial facilities. Each concrete slab was of the same composition made of the same batch, which is provided in

Table 3. The setups were instrumented using eight thermocouples and two heat flux sensors as shown in Figure 17. The location of the thermocouples and heat flux sensors with respect to the reference point (shown in Figure 17) are provided in Table 11 in Section 0. For good thermal contact, high conductive thermal paste from Omega was used to fill the gap between the two slabs of concrete. The walls were made of stainless steel, 1 mm thick sheets, which created 100 mm walls above the top surface. The low-temperature silicone sealant was used to make sure the setup was leak resistant and the rebars and wooden wedges were used to press and support the walls (see Figure 35 in Section 0). One heat flux sensor was attached using high conductive thermal paste to the outer side of wall to measure the wall heat flux. There were four thermocouples placed at the top surface of upper slab to monitor the temperature of the cryogen.

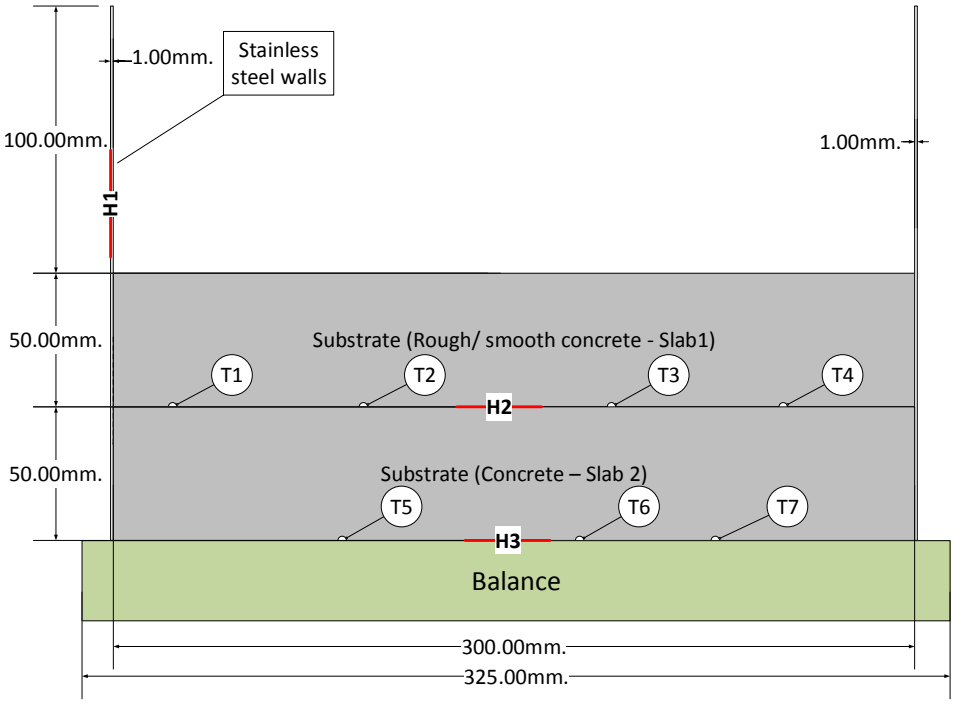

Figure 17: Rough/smooth surface concrete base setup (H1-H3 are the heat flux sensors and T1-T8 are the thermocouples; all dimensions mentioned in mm)

Table 3: Composition of concrete

Material	Batch Weight (kg m^{-3})	Fraction (% kg m^{-3})	Mass proportion rel. to C
Dry Portland cement (C)	380	15.6	1
Aggregate 20 mm (A)	676	27.75	3
Aggregate 10 mm (A)	451	18.52	
Washed Sand (S)	766	31.45	2
SP495 (L m^{-3})	7.6	0.31	
Water (L m^{-3})	155	6.36	0.4
Designed density	2435.6	100	
*prepared by Societe d'Entreprise & de Gestion - Qatar W.L.L. Company			

After the preparation of the setups, the roughness of the complete surface was measured as described in Section 0 . The average roughness of the rough and smooth concrete surface were 39.8 µm and 9.0 µm, respectively (Table 4). It was noted that the standard deviation for smooth surface concrete is much higher (in relative term) than that of the rough one. This effect might be due to the presence of very smooth rocks at the surface of the smooth concrete, which became exposed during the polishing process. Nearly 30% of the surface of smooth concrete is covered with rocks that are very smooth and have an average roughness of as low as 2.9 µm (Figure 18).

Table 4: Surface roughness of concrete base setup

Concrete surface type	Average roughness (µm)	Standard Deviation (µm)
Rough concrete surface	39.8	5.1
Smooth concrete surface	9.0	4.7
Very smooth rocks	2.9	1.0

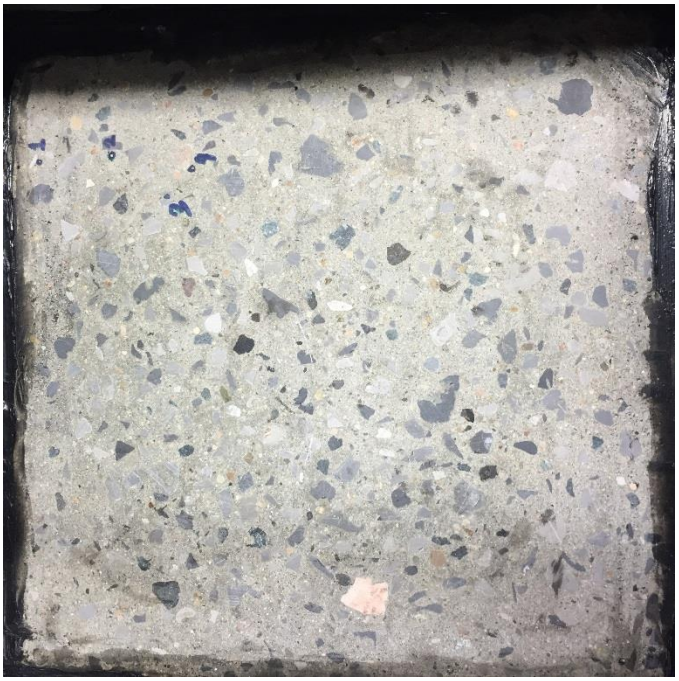

Figure 18: A photograph of smooth surface concrete slab covered with rocks

Experiments on both rough and smooth concrete are conducted by spilling cryogenic liquids into the setups and refilling before the box is empty. In the case of liquid nitrogen/oxygen mixture experiments, an oxygen sensor (described in Section 0) was used to determine the oxygen concentration in the headspace vapor of the binary liquid contained in the Dewar. The recorded concentration is then used to determine the oxygen concentration in the liquid phase using Vapor-Liquid Equilibrium (VLE) calculations (also described in Section 0).

5.2 Steel base

The steel base setup was built using a carbon steel plate of dimension 300 mm x 300 mm x 24 mm. The plate was milled using Computer Numerical Control (CNC) machine in Texas A&M University at Qatar's machine shop. After the milling process, the plate was drilled, to instrument it with eight thermocouples. The precise location of the thermocouples with respect to the reference point (shown in Figure 19) are provided in Table 12 and Figure 36 in Section 0. After drilling the steel plate, steel walls of height 100 mm and 1 mm thickness were welded on all four sides of the plat, which created a 100 mm wall above the top surface. One heat flux sensor was attached to the wall using high conductive thermal paste to measure the wall heat flux. There were two thermocouples placed at the top surface of the base to monitor the temperature of the cryogen.

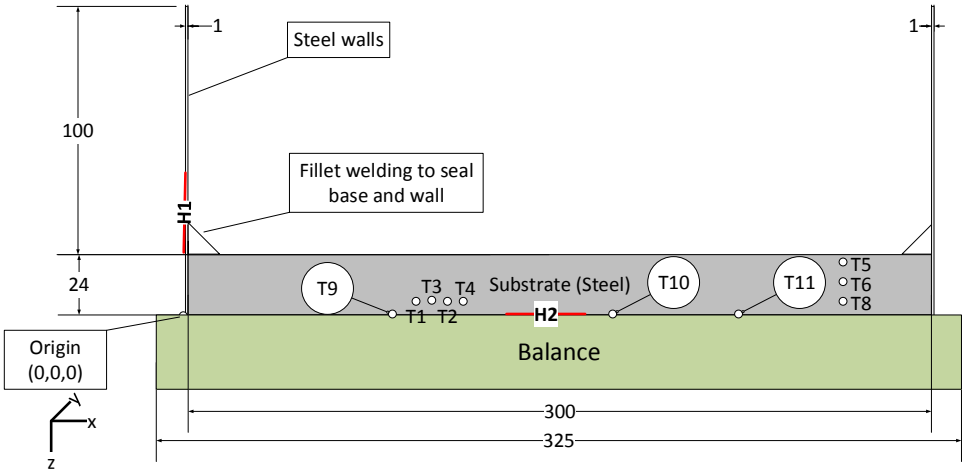

Figure 19: Steel base setup (H1 is the heat flux sensor and T1-T8 are the thermocouples; all dimensions mentioned in mm)

5.3 Polystyrene base

The polystyrene base setup (Figure 20) was built using 50 mm thick polystyrene sheets. The base was built using three sheets of polystyrene of dimension 400 mm x 400 mm x 50 mm stacked on top of each other. Each side of the wall was built by placing three sheets of polystyrene, which created 100 x 100 mm and 150 mm deep container for the liquid on top of the base. Before stacking the sheets, the seventeen thermocouples and three heat flux sensors were instrumented with high conductive thermal paste manufactured by Omega. The position of each sensor with respect to the reference point (shown in Figure 20) is provided in Table 13 in Section 0. The gaps between the adjacent sheets were sealed using a low-temperature silicone. There were fifteen thermocouples placed at different distance above the top surface of the base to monitor the temperature of the cryogenic pool.

The experimental procedure includes blank test (without liquid) runs at four different wind speeds of 0 m s^{-1}, 3.5 m s^{-1}, 4.3 m s^{-1} and 4.9 m s^{-1} to determine the sensitivity of the balance to the changing fan speed. The experiment was then carried out with liquid nitrogen spill into the box at the same wind speeds as in blank tests. The refills of the liquid were accompanied by change of fan speed. There was a total of four fills, one for each fan speed.

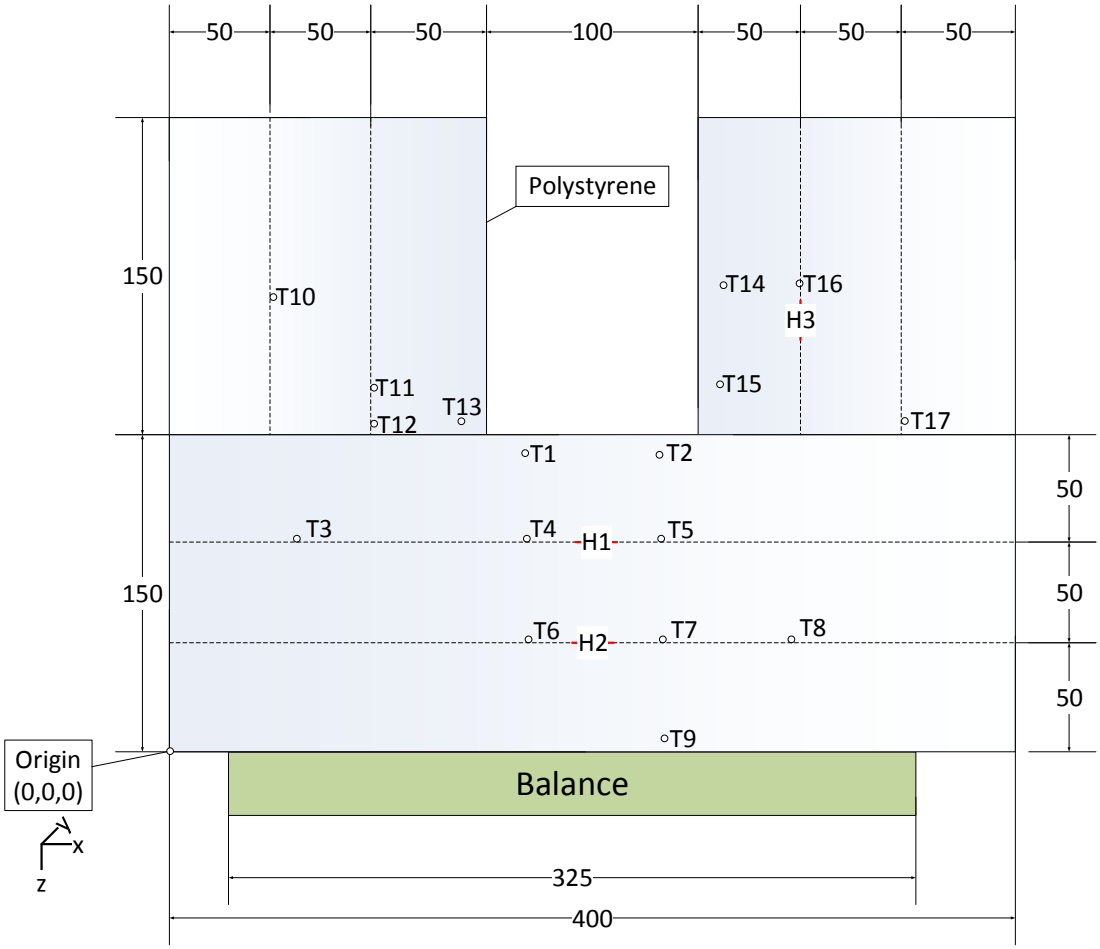

Figure 20: Polystyrene setup (H1-H3 are the heat flux sensors; T1-T17 are the thermocouples; all dimensions mentioned in mm)

5.4 Thermal properties of concrete

To incorporate the temperature-dependent thermal properties of concrete in to the models, two concrete slabs were sent to NETZSCH to obtain the thermal conductivity (using GHP technique) and heat capacity (using DSC technique) as a function of temperature. The result of this analysis is shown in Figure 21. The graph shows that heat capacity of concrete increases with temperature that is consistent with literature [48,49] as

shown in Figure 23. However, the increase in thermal conductivity of concrete with temperature is not consistent with few literature sources [49,50] as shown in Figure 22. This may be due to the composition of the concrete. The exact reason cannot be pointed out and hence, will be investigated in the future.

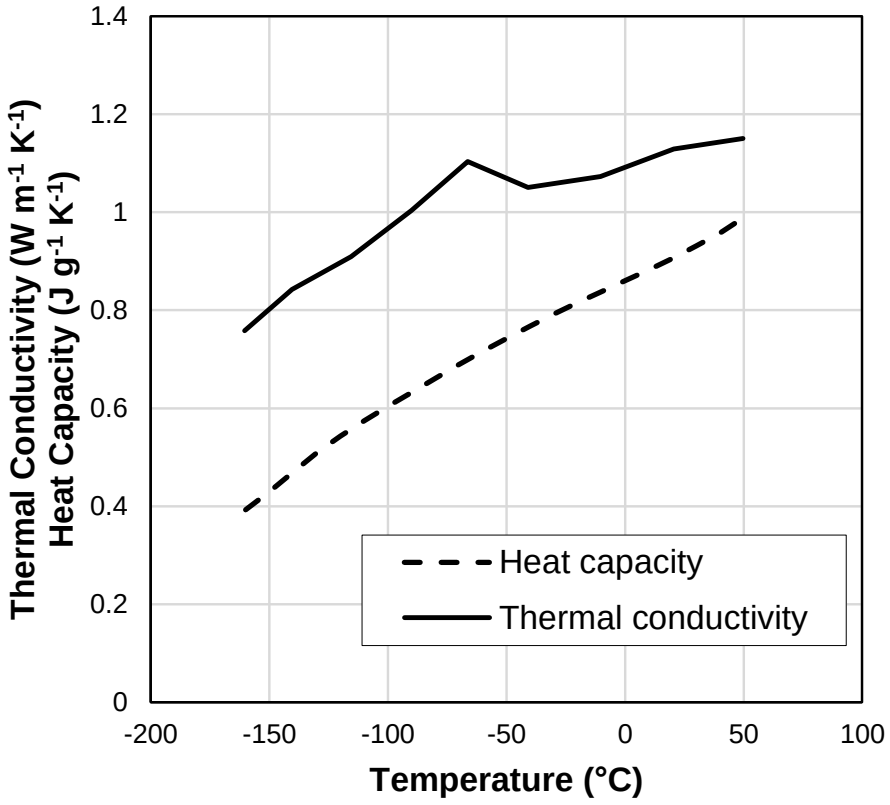

Figure 21: Thermal conductivity and heat capacity of used concrete as a function of temperature

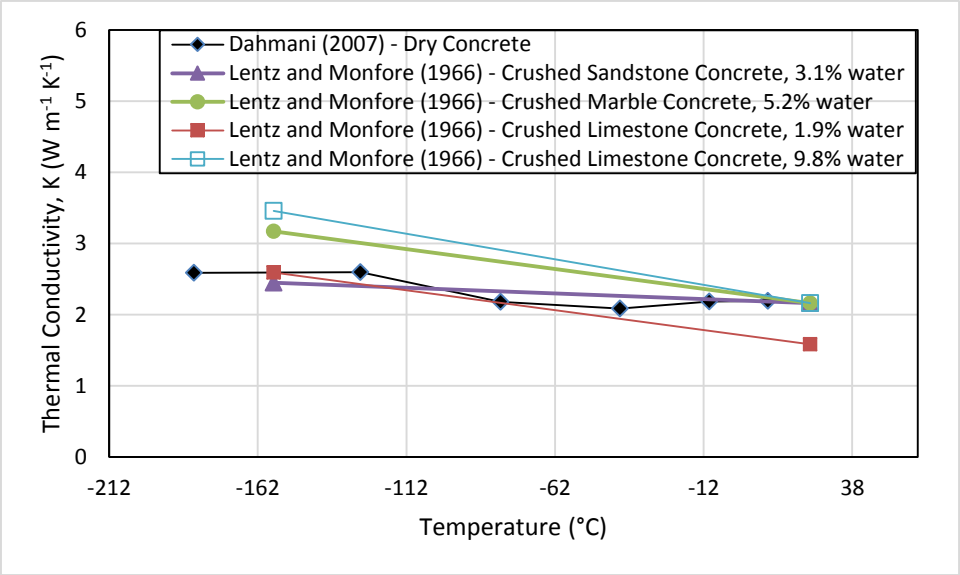

Figure 22: Variable thermal conductivity of concrete with temperature and water content [49,50]

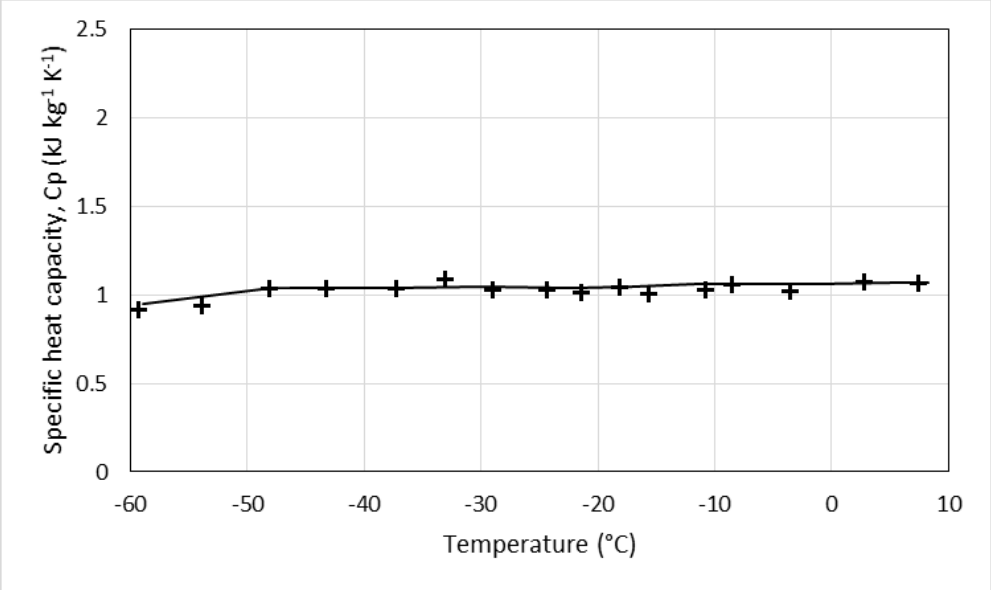

Figure 23: Variable specific heat capacity of concrete with temperature [49]

5.5 Challenges encountered

Each of the laboratory scale experiments mentioned above were designed, instrumented and built to achieve the corresponding objectives. The following were the challenges encountered when preparing the final setup and conducting experiments in each case:

- The silicone sealant was used to seal the gaps between walls and base, however it was very challenging to keep the setup leak-proof. The cryogenic liquid spill caused the sealant to shrink, resulting in widening of the gaps, which in turn led to leakage. This happened every time a setup was built. Each time, the setup was dismantled and reassembled again with minor changes in the design. The process of learning with practice was heavily time consuming and required constant effort to achieve the goals of the experiment.
- An international vendor was contacted to obtain a Dewar that can contain liquid nitrogen/oxygen mixture. This task of preparing the Dewar as per the request, shipping it to Qatar and clearing the Qatar customs took 4 months.

6. RESULTS AND ANALYSIS

The experimental results obtained through a series of runs (Table 5) on different types of substrates with pure and binary cryogens were analyzed to study:

- The effect of concrete surface roughness on vaporization rate of liquid nitrogen.
- The effect of type of solid substrate (concrete and steel) on the vaporization rate of liquid nitrogen.
- The effect of type of cryogen (pure or binary mixture) on their vaporization rate on smooth surface concrete.
- The validation of 1D conduction model and boiling regimes model for cryogenic spills on solid surface.
- The transition from boiling to evaporation regime of cryogenic liquid.

Table 5: List of total runs conducted for each experiment and their status

Cryogen	Substrate	Run No.	Status
LN2	Rough surface concrete	Run 1	Failure
		Run 2	Failure
		Run 3	Success
		Run 4	Success
		Run 5	Success
	Smooth surface concrete	Run 1	Failure
		Run 2	Failure
		Run 3	Failure
		Run 4	Failure
		Run 5	Failure
		Run 6	Failure
		Run 7	Success
		Run 8	Success
		Run 9	Success
	Steel	Run 1	Success
		Run 2	Success
LN2/O2	Smooth concrete	Run 1	Success
		Run 2	Failure
		Run 3	Success
		Run 4	Success
LN2	Polystyrene	Run 1	Success
		Run 2	Success
		Run 3	Success

6.1 The effect of concrete surface roughness on vaporization rate of liquid nitrogen and the validation of models

There were two concrete base setups prepared to study the effect of substrate surface roughness on vaporization rate of liquid nitrogen: smooth and rough. There were five runs performed on rough surface concrete base and three were successful. In the case of smooth surface concrete base, there were nine runs performed and three were successful. The vaporization rate as a function of time for the three successful runs, on rough and smooth surface concrete are shown in Figure 24 and Figure 25, respectively. All the runs show no significant difference between the runs and good repeatability (see also Table 6).

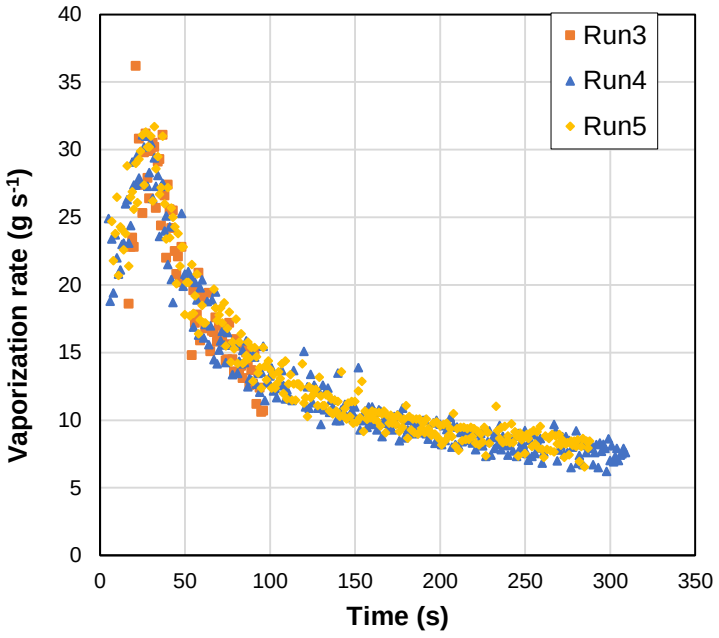

Figure 24: Repeatability of LN_2 experiments on rough concrete surface

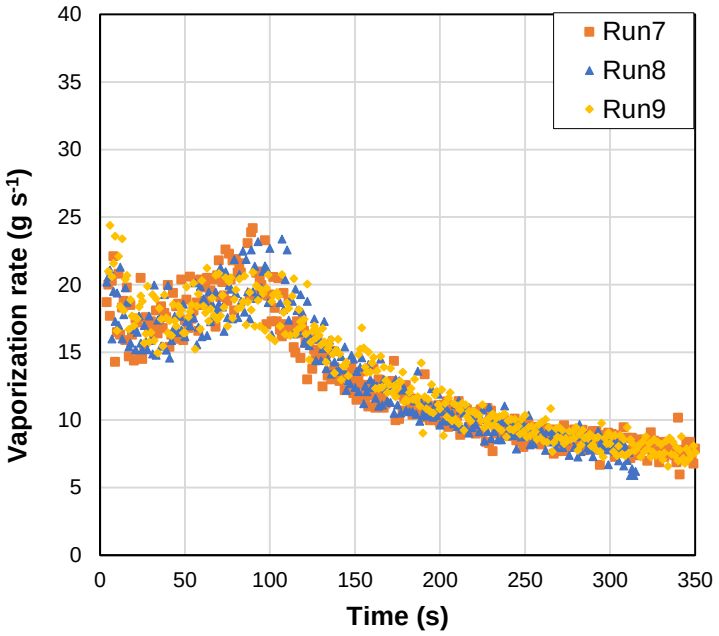

Figure 25: Repeatability of LN_2 experiments on smooth concrete surface

The temperature measurements of three thermocouples placed at each depth of 0 mm, 50 mm and 100 mm and at different horizontal distances are shown in Figure 26. At each depth, the three measurements showed the same reading regardless the horizontal position, thereby showing, both, uniform liquid spill (temperatures at 0 mm) and uniform vertical temperature profile (temperatures at 50 and 100 mm). The first shows uniform and quick distribution of liquid during spill and the second shows negligible effect of potential heat flux from the sides.

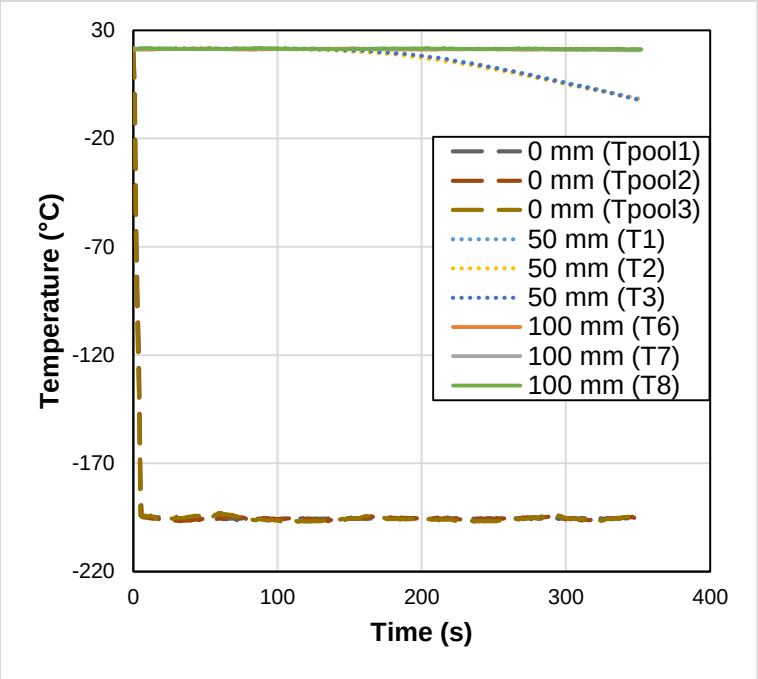

Figure 26: Temperature profile in the concrete setup at different depths (from the boiling surface) and pool temperature during LN2 spill on concrete

Two boiling regimes, transition and nucleate boiling, were observed during the spill on rough surface (Figure 24). The transition regime lasted for about 25 s from the start of the spill and the maximum vaporization rate of 31.33 g s^{-1} (average of all runs) was reached. The heat flux at this time is called critical heat flux (CHF). The average value of CHF for all the runs was 69.27 kW m^{-2}. After the CHF point, the vaporization rate and consequently, the heat flux from the ground decreases indicating nucleate boiling. Although film boiling regime was not observed in the rough surface concrete experiments, it is important to note that the presence of this regime cannot be completely disregarded. If this regime existed, then it is in the first 5 seconds of the cryogenic liquid spill as this was the time of the fill, at which data could not be collected.

Unlike for rough surface, all three boiling regime: film, transition and nucleate boiling, were observed during the spill over smooth surface (Figure 25). The film boiling regime was observed for about 20 s from the start of the spill. The minimum vaporization rate at Leidenfrost point was determined and the value was 14.61 g s^{-1} (average of all runs), which corresponds to 32.31 kW m^{-2} of heat flux. After 20 s the transition regime was observed that lasted until 90 s from the start of the spill. The maximum vaporization rate reached at 90 s was 24.02 g s^{-1} (average of all runs). After this time a shift of boiling regime from transition to nucleate was observed. The CHF corresponding to this point was 52.99 kW m^{-2}. At about 90 s the nucleate regime started and continued until the end of the experiment, which lasted for about 300 – 350 seconds.

The heat flux as a function of time for LN_2 spill on smooth surface concrete is shifted to the right of that on rough concrete surface (shown in Figure 27). The onset of nucleate boiling regime was delayed on smooth concrete surface. The CHF was found to be smaller (shown in Figure 27 and Table 6) as roughness of the concrete decreased. This was observed by Bui and Dhir [32] for boiling of water (see Figure 8). This shows that the surface roughness effects on CHF for cryogens and non-cryogenic liquids is the same. These observations also confirmed Bui and Dhir's [32] contradiction to Berenson's [24] conclusion that CHF is independent of surface roughness. The difference of the CHF values between liquid nitrogen experiments on rough and smooth surface is calculated to be 26.63 %. This difference is much higher than the difference calculated by Berenson, which was about 10 % [24]. Because of this small difference (10 %), he assumed it as not significant and concluded that the CHF value was independent of surface roughness owing

to the engineering considerations. However, the observations made in this experiment clearly confirms that CHF value increases with surface roughness and this effect can be strong enough to not be neglected.

At a particular time, the heat flux in the nucleate boiling regime was found to be smaller when surface roughness increased. The film boiling regime was observed on smooth surface concrete only. As a result, if there was film boiling regime present on rough surface concrete, it would not have followed the same path as smooth surface concrete. This implies that the film boiling regime is not independent of surface roughness effect, which contradicts Berenson's [24] and Bui and Dhir's [32] conclusions made based on non-cryogen boiling and on surfaces that have rather small roughness, unlike concrete. In our case, spill of cryogenic liquid on very rough surface, the film boiling regime was function of roughness.

The comparison of the 1D and boiling regimes model with the experimental results (2 s average) is shown in Figure 27. It is important to note that in order to validate 1D conduction model, the experimental data can be used only if the temperature of the bottom of the base is constant, which is true in our experiment for about 350 seconds (see Figure 26). As mentioned in Section 4.2.2, the 1D model was evaluated at χ=1 and χ=3 (Figure 27). The value of 3 was suggested by Briscoe and Shaw [10] to match the theoretical predictions of their model with the experimental data that they used to compare with. As shown in Figure 27, the model at χ=3 do not represent the experimental data correctly. However, the experimental results do fall in the region between the model with χ=3 and evaluated with concrete temperature at T_i and that evaluated with concrete temperature at

T_b (Figure 27). On the other hand, when the model was evaluated without accounting for surface roughness (χ=1), the experimental results was significantly under predicted. It is concluded that the model with χ parameter different than 1 could fit experimental results. This shows that surface roughness (and maybe other parameters) is an important parameter that needs to be incorporated into the model.

Similar to 1D model with χ equal to 1, the boiling regimes model also severely under predicted the experimental results. It seems obvious that this model could also be easily improved if χ parameter was incorporated here, although the question can be raised if all the complication associated to this model is then needed. This should be discovered and analyzed in the future work, and the experimental work provided in this thesis could provide a basis for analysis and future models improvements.

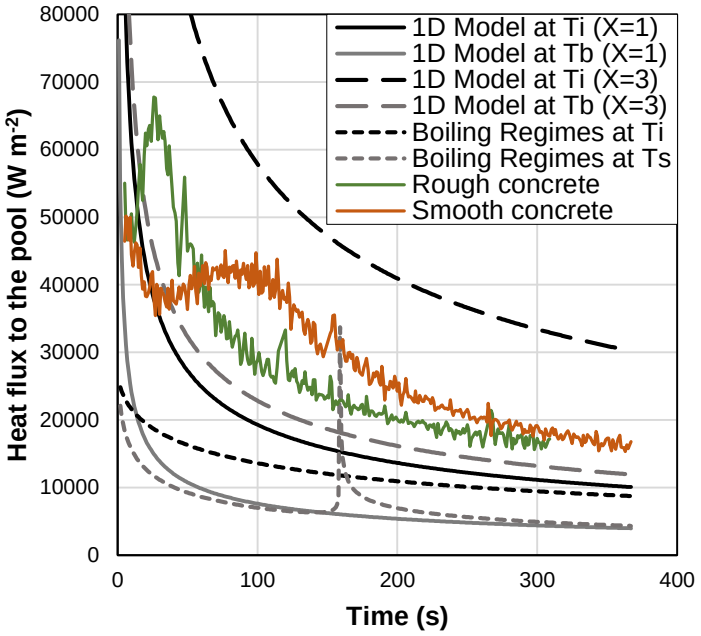

Figure 27: Comparison of rough and smooth surface concrete experiments with the 1D and boiling regimes model

Table 6: CHF and Leidenfrost values of boiling of LN2 on smooth and rough surface concrete

Smooth surface concrete				
Run no.	Vaporization rate at CHF ($g\ s^{-1}$)	CHF ($kW\ m^{-2}$)	Vaporization rate at Leidenfrost ($g\ s^{-1}$)	Leidenfrost heat flux ($kW\ m^{-2}$)
Run7	24.12	53.33	14.30	31.62
Run8	23.38	51.69	14.57	32.21
Run9	24.40	53.95	14.96	33.09
Average	23.96	52.99	14.61	32.31
Rough surface concrete				
Run no.	Vaporization rate at CHF ($g\ s^{-1}$)	CHF ($kW\ m^{-2}$)	Vaporization rate at Leidenfrost ($g\ s^{-1}$)	Leidenfrost heat flux ($kW\ m^{-2}$)
Run 3	31.20	68.98	N/A	N/A
Run 4	31.10	68.76		
Run 5	31.69	70.07		
Average	31.33	69.27		

6.2 The effect of type of solid substrate (concrete and steel) on the vaporization rate of liquid nitrogen

The steel base was used to perform the experiments with liquid nitrogen spills and the result was compared to these of concrete. There were two runs performed and both were successful. The vaporization rate as a function of time for both the runs are shown in Figure 28. The first run consisted of one spill and the second consisted of three refills. The repeatability of initial stage of film boiling was very good (first 115 seconds in Figure

28). However, it is clear that repeatability during these experiments is not very good upon liquid refill during which the film was broken. The film boiling of the Run 1 was about 190 s and last till the liquid was still present in the box, whereas it was much shorter during the Run 2 and its breakup overlap exactly with the refill (see Figure 28). At about 320 s of Run 2, there was a second refill, which interrupted the transition boiling (raising heat flux) and the boiling shifted from transition to nucleate boiling regime. After about 600 s, the steel is cold enough to switch to convective boiling and very slow vaporization.

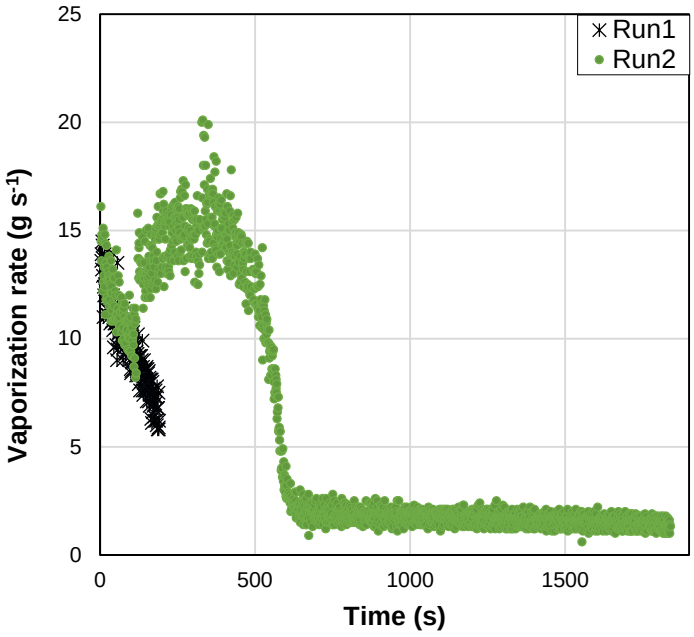

Figure 28: Repeatability of LN_2 experiments on steel plate

Although, a maximum for the vaporization rate was observed, this point cannot be used for the calculation of CHF since it exactly overlap with the refill and might be

affected by this. As a result, only the film boiling regime of this experiment can be used for future model validation.

The temperature profile at the given depths (from the boiling surface) in the steel plate and the temperature of the pool are shown in Figure 29. There is no significant differences in the temperature at different depths of the steel plate and it is clear that the temperature at the base change very quickly with time, which was expected as the steel plate has high thermal conductivity. Therefore, the use of this data for validation of 1D model is very limited since the temperature of the bottom of the base changes in just 14 seconds (so short that not even seen in Figure 29). Therefore, the vaporization rate graph for steel (Figure 28) cannot be directly compared to the one obtained on concrete (Figure 24 and Figure 25), however it is obvious that the film and transition boiling regimes are much longer on steel than on concrete.

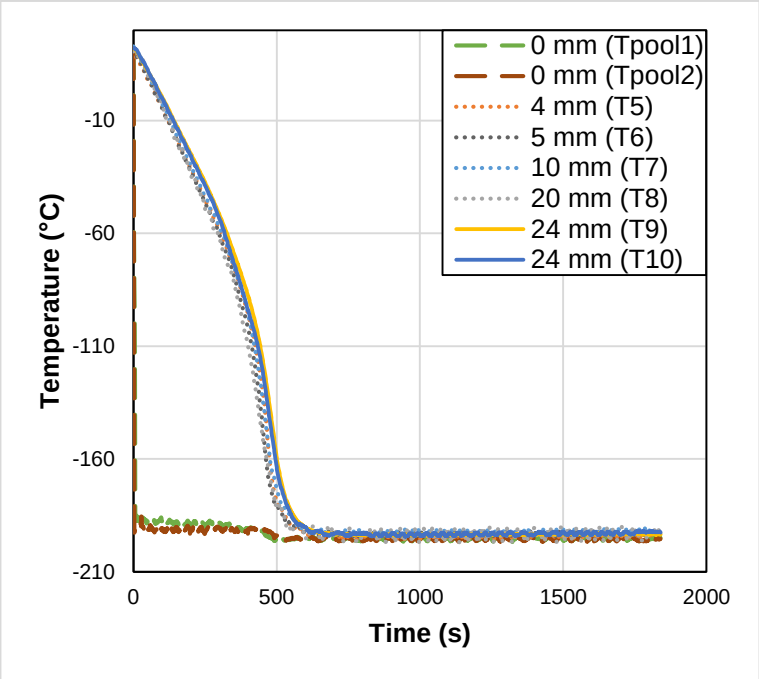

Figure 29: Temperature profile in the steel setup at different depths (from the boiling surface) and pool temperature during LN_2 spill on steel

6.3 Binary mixture effect on smooth concrete

The difference between pure (liquid nitrogen) and binary mixture (liquid nitrogen/oxygen mixture) vaporization rate is studied on smooth concrete. There were four runs performed with binary mixture in addition to these described in section 6.1 and three runs were successful. The vaporization rate as a function of time for all the runs are shown in Figure 30. Since there was no significant difference observed between the three runs, the experimental results were concluded repeatable. The repeatability is also confirmed by CHF and Leidenfrost values for all the runs of liquid nitrogen/oxygen mixture spill on smooth surface concrete provided in Table 7. The presence of all the three regimes in the

boiling of the mixture on smooth surface concrete was observed and is shown in Figure 30.

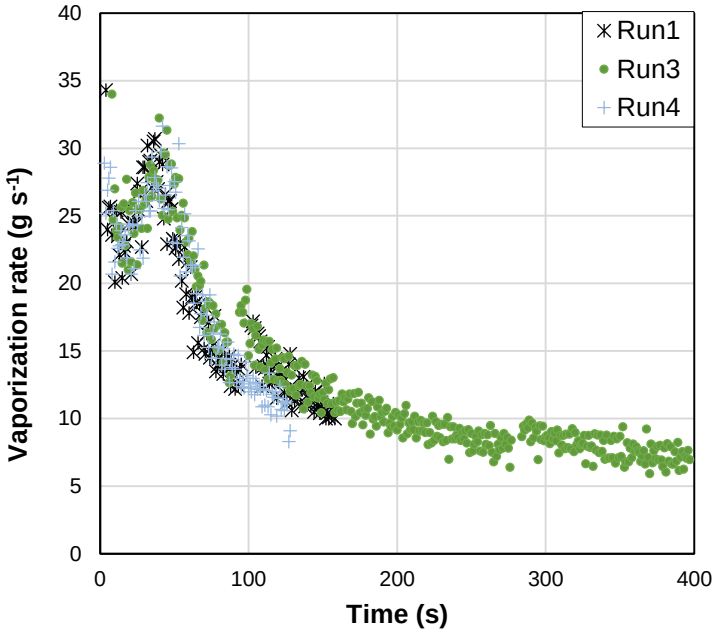

Figure 30: Repeatability of LN_2/O_2 experiments on smooth concrete surface

The composition of the mixture was measured before the experiment. The liquid mixture contained 46 % oxygen and the rest was nitrogen. It is obvious that due to the preferential boil off of liquid nitrogen, which vaporize faster, the composition during the lifetime of the pool change, which is reflected in change of its temperature (Figure 31). The pool is initially at the boiling temperature of the mixture (above the boiling point of nitrogen) and then it changes to the boiling point of oxygen as nitrogen vaporizes and the concentration of oxygen in the remaining pool increases.

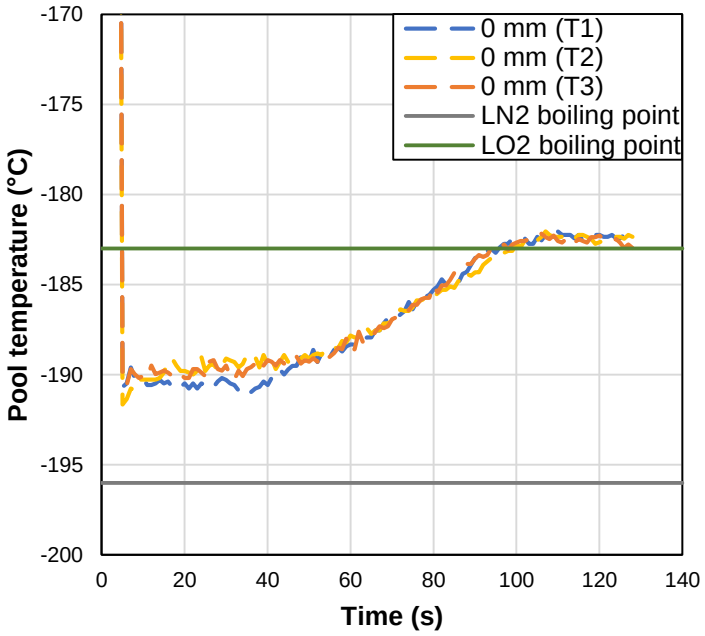

Figure 31: Pool temperature during LN_2/O_2 spill on smooth surface concrete

Drake et al. [51] studied the boiling of LNG and methane on water. They showed that LNG, being a mixture, had faster vaporization rate when compared to pure methane. The experimental results obtained in this work is in agreement with the results obtained by Drake et al. [51]. This can be seen in Figure 32 where the vaporization rate of the liquid nitrogen/oxygen mixture is faster than pure nitrogen (shown as mass vaporized).

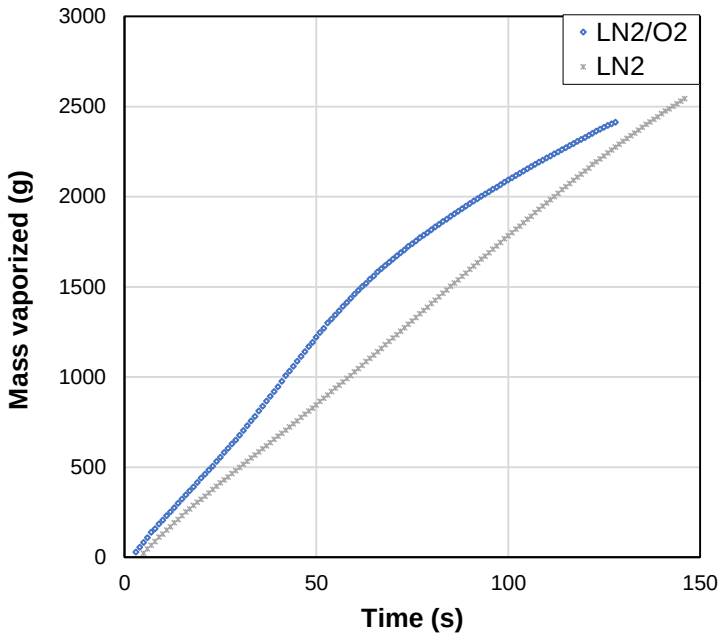

Figure 32: Mass vaporized of pure and binary mixture on smooth surface concrete

Both of the liquids, pure liquid nitrogen and its mixture with oxygen, boil in all three regimes of boiling (Figure 33). The binary mixture is characterized by higher heat flux delivered at the film boiling regime. Both, the CHF and Leidenfrost point of the binary mixture are higher than that of pure liquid. The film boiling duration seems to be only slightly shorter for binary mixture, whereas the transition boiling duration is significantly shorter.

The experimental results of this work can greatly contribute to the improvement of models that can predict the vaporization of cryogenic mixtures.

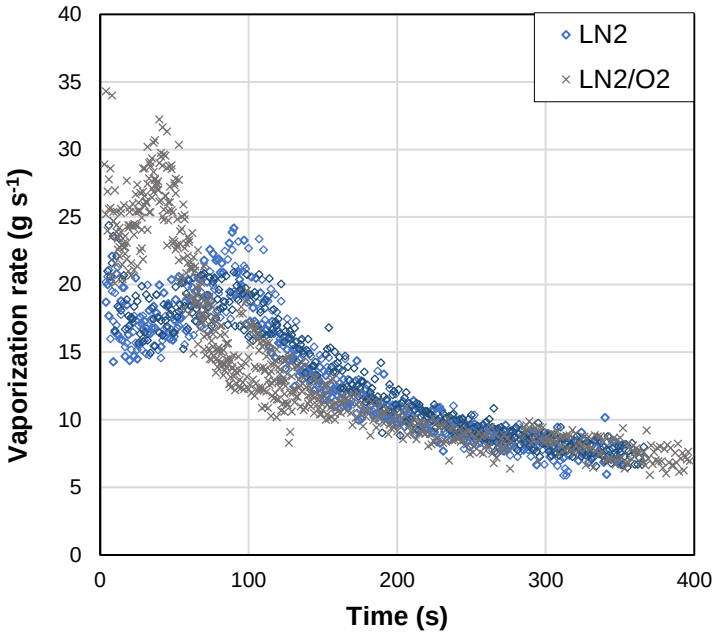

Figure 33: The vaporization of pure and binary mixture on smooth surface concrete

Table 7: CHF and Leidenfrost values of boiling of LN_2 and LN_2/O_2 on smooth surface concrete

LN2 on smooth surface concrete				
Run no.	Vaporization rate at CHF ($g\ s^{-1}$)	CHF ($kW\ m^{-2}$)	Vaporization rate at Leidenfrost ($g\ s^{-1}$)	Leidenfrost heat flux ($kW\ m^{-2}$)
Run7	24.12	53.33	14.30	31.62
Run8	23.38	51.69	14.57	32.21
Run9	24.40	53.95	14.96	33.09
Average	23.96	52.99	14.61	32.31
LN2/O2 on smooth surface concrete				
Run no.	Vaporization rate at CHF ($g\ s^{-1}$)	CHF ($kW\ m^{-2}$)	Vaporization rate at Leidenfrost ($g\ s^{-1}$)	Leidenfrost heat flux ($kW\ m^{-2}$)
Run 1	30.70	67.88	20.10	44.44
Run 3	32.24	71.29	20.99	46.41
Run 4	31.65	69.98	20.69	45.74
Average	31.53	69.72	20.59	45.53

6.4 The determination of the transition from boiling to evaporation regime of cryogenic liquid spilled on solid substrate

The polystyrene base experiment is designed to study the transition from boiling to evaporation regime when liquid nitrogen is spilled on polystyrene. There were three runs performed and all of them were successful. The repeatability of the data can be seen in Figure 34. The wind speeds were varied from 0-5 $m\ s^{-1}$ in each run. The temperature of the pool was always at the boiling point of liquid nitrogen with varying wind speeds during

each run (Figure 34). Therefore, evaporation was not observed in the polystyrene experiment.

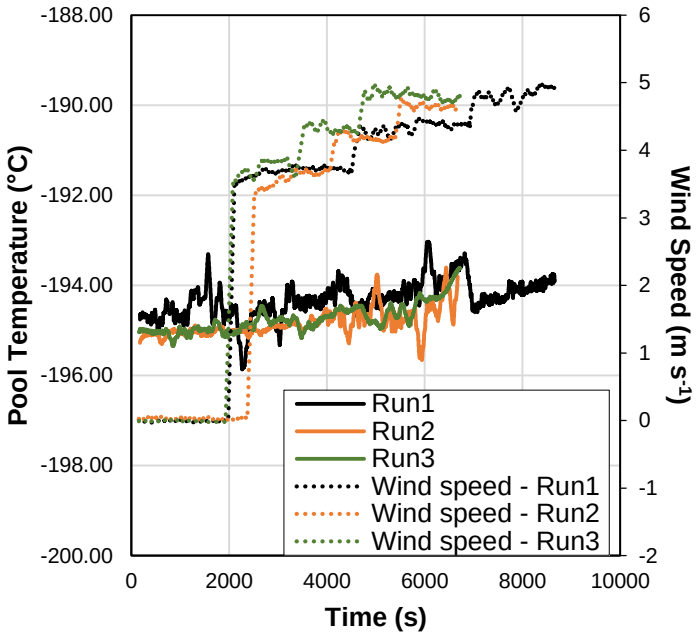

Figure 34: Pool temperature vs time at different wind speeds during the polystyrene base experiment

7. CONCLUSION AND FUTURE WORK

An extensive literature survey on the boiling phenomena of LNG spill on a solid substrate and its modeling was conducted. The available literature showed that the boiling phenomena were studied using non-cryogenic liquids and consequently, models, such as 1D conduction model and boiling regimes model were formulated and also adopted for cryogenic liquids. This work raised the question whether this approach is acceptable and there is a need for improvement of such models to represent cryogenic liquids. Thus, the study to generate broad range of experimental data that can be used for models validation was proposed.

In this work, experimental data was generated for spill of liquid nitrogen on different solid substrates: concrete and steel to study the effect of type of substrates on cryogenic boiling. The effect of the pool composition (using liquid nitrogen – pure and liquid nitrogen/oxygen mixture – binary) and surface roughness (rough and smooth surface) was studied on concrete. An attempt was made at studying the transition from boiling to evaporation regime of liquid nitrogen boiling on polystyrene (conduction limited). The experimental data of liquid nitrogen spill on rough and smooth surface concrete was compared with 1D conduction and boiling regimes models.

The experimental results and their comparison to the models provided the following key findings:

- The surface roughness effect on the boiling rate of liquid nitrogen on concrete were consistent with some of the findings of Bui and Dhir [32] that was based

on non-cryogenic liquid. The heat flux as a function of time of rough concrete shifted to the left of that of smooth concrete. The experimental results also contradicted Berenson's [24] conclusion that CHF is unaffected by surface roughness. This finding was earlier refuted in Bui and Dhir's [32] conclusion. The results confirmed Bui and Dhir's [32] assertion that CHF increases when surface roughness increases. Since, film boiling was not observed for liquid nitrogen spill on rough surface concrete, the Leidenfrost point was not determined. However, it can be concluded that, in this case, the Leidenfrost point is different for both rough and smooth surface concrete. This is different from the observations made by Berenson [24] and Bui and Dhir [32] that the film boiling regime is the same regardless of surface roughness.

- The existing models, 1D and boiling regimes, were proved to be not in good agreement with the experimental results. Both models seem to severely under predict the heat flux as a function of time of the experimental results. One reason could be attributed to the models not accounting for the surface roughness and they need correction factors. Such factor has been applied to 1D model and the value of χ=3 was utilized as suggested by Briscoe and Shaw [10]. However, it was shown that value of 3 is too high to apply for the results of this work and need to be separately quantified to accurately represent the experimental data.
- It was shown that the effect of composition of a binary mixture (liquid nitrogen/oxygen mixture) on its boiling rate was in good agreement with

Drake et al. [51]. The film and transition boiling regime of the binary mixture had a higher heat flux than that of the pure liquid (liquid nitrogen). The CHF and Leidenfrost point observed in this work were higher for binary mixture than that for pure liquid.

- The liquid nitrogen spill on polystyrene base did not show any transition to evaporation regime with varying wind speeds.

The experimental work performed in this work were carefully designed to meet the objectives of studying the effect of type of substrate, mixture composition and surface roughness on cryogenic liquid boiling. However, small improvements can be made to the experimental setup in order to increase quality of data. The use of polystyrene to insulate the walls could have reduced their effect allowing for smaller deviations.

Although these experimental results could be used for model validation and improvements, it is important to consider scaling up of these experiments in order to take the scale effect into consideration. An extension of this work, with medium and large scale experiments, performed specifically for concrete, would be desirable.

REFERENCES

1. BP Statistical Review of World Energy June 2014. 2014;(June). Available at: http://www.bp.com/content/dam/bp/pdf/Energy-economics/statistical-review-2014/BP-statistical-review-of-world-energy-2014-full-report.pdf.

2. Liquefied Natural Gas exports-America's Opportunity and Advantage. 2014;(March). Available at: http://www.api.org/policy-and-issues/policy-items/lng-exports/~/media/Files/Policy/LNG-Exports/LNG-primer/Liquefied-Natural-Gas-exports-lowres.pdf.

3. Liu Y, Guo K. A novel cryogenic power cycle for LNG cold energy recovery. *Energy*. 2011;36(5):2828-2833. doi:10.1016/j.energy.2011.02.024.

4. Webber D, Gant S, Jagger S. *LNG Source Term Models for Hazard Analysis: A Review of the State-of-the-Art and an Approach to Model Assessment*. Buxton, Derbyshire, UK; 2010.

5. Woodward JL, Pitblado R. *LNG Risk Based Safety - Modeling and Consequence Analysis*. Hoboken, NJ, USA; Published simultaneously in Canada: AIChE, John Wiley & Sons, Inc.; 2012:374.

6. Qatar LNG vessel involved in collision. *Arabian Oil and Gas*. http://www.arabianoilandgas.com/article-11636-qatar-lng-vessel-involved-in-collision/. Published January 7, 2014.

7. United States Government Accountability Office. *Report GAO-07-633T - Public Safety Consequences of a Liquefied Natural Gas Spill Need Clarification Clarification.*; 2007. Available at: http://www.gao.gov/assets/120/115926.pdf.

8. Woodward JL, Pitblado RM. *LNG Risk Based Safety - Modeling and Consequence Analysis*. John Wiley & Sons, Inc.; 2012.

9. Olewski T, Véchot L, Mannan MS. Study of the Vaporization Rate of Liquid Nitrogen by Small- and Medium-Scale Experiments. Rademaeker E De, Fabiano B, Buratti SS, eds. *Chem Eng Trans*. 2013;31(1):133-138. Available at: http://www.aidic.it/cet/.

10. Briscoe F, Shaw P. Spread and Evaporation of Liquid. *Prog Energy Combust Sci*. 1980;6(2):127-140.

11. Moorhouse J, Carpenter RJ. Factors affecting vapour evolution rates from liquefied gas spills. *North West Branch Pap Inst Chem Eng*. 1986;1:4.1-4.18.

12. Olewski T, Vechot NL, Mannan S. Validation of Liquid Nitrogen Vaporisation Rate by Small Scale Experiments and Analysis of the Conductive Heat Flux from the Concrete. In: *Hazards Asia Pacific Symposium*.; 2013.

13. Burgess DS, Zabetakis MG. *Fire and Explosion Hazards Associated with Liquefied Natural Gas, US Bureau of Mines Report of Investigations No. 6099*.; 1962.

14. American Gas Association. *LNG Safety Program: Interim Report on Phase II Work*. Columbus, Ohio, USA: American Gas Association; 1974.

15. Nukiyama S. The maximum and minimum values of the heat Q transmitted from metal to boiling water under atmospheric pressure. *Int J Heat Mass Transf*. 1966;9(12):1419-1434. Available at: http://dx.doi.org/10.1016/0017-9310(66)90138-4.

16. Boe R. Pool boiling of hydrocarbon mixtures on water (Thesis). 1996.

17. Sakurai a, Shiotsu M, Hata K, Fukuda K. Photographic study on transitions from non-boiling and nucleate boiling regime to film boiling due to increasing heat inputs in liquid nitrogen and water. *Nucl Eng Des*. 2000;200(1-2):39-54. doi:10.1016/S0029-5493(99)00325-8.

18. Nicholds KE. Leidenfrost. *Cryogenics (Guildf)*. 1970;(February):45-47.

19. Bankoff SG. Entrapment of gas in the spreading of a liquid over a rough surface. *AIChE J*. 1958;4(1):24-26. doi:10.1002/aic.690040105.

20. H. B. C, P. S. S, J. W. W. Active sites for nucleation. *Chem Eng Prog Symp Ser*. 1959;55:103-110.

21. Dhir V. Nucleate and transition boiling heat transfer under pool and external flow conditions. *Int J Heat Fluid Flow*. 1991;12(4):290-314.

22. Liu Y, Olewski T, Vechot L, Gao X, Mannan S. Modelling of a cryogenic liquid pool boiling using CFD code. In: *14th Annual Symposium, Mary Kay O'Connor Process Safety Center "Beyond Regulatory Compliance: Making Safety Second Nature."* College Station, TX, USA; 2011:512-524.

23. Dhir VK. Boiling Heat Transfer. *Annu Rev Fluid Mech*. 1998;30(1):365-401. doi:10.1146/annurev.fluid.30.1.365.

24. Berenson PJ. Experiments on pool-boiling heat transfer. *Int J Heat Mass Transf*. 1962;5:985-999.

25. Kalinin EK, Berlin II, Kostyuk V V, Nosova EM. Heat transfer in transition boiling of cryogenic liquids. *Adv Cryog Eng*. 1976;21:273-277.

26. Gregoryev VA, Pavlov YM, Ametistov E V. Teploenergetika. *Teploenergetika*. 1973;(9):57.

27. Kalinin EK, Berlin II, Karavayev VG, Kostyuk V V., Nosova EM. Inzhenerno. *Inzhenerno-fizicheskii Zh*.

28. Kalinin EK, Berlin II, Kostyuk V V., Podzei I V. No Title. *Inzhenerno-fizicheskii Zh*. 1973;(25):205.

29. Kutateladze SS. Heat Transfer in Condensation and Boiling. *Energia*. 1952.

30. Gopalaswami N, Mannan MS, Véchot LN, Olewski T. Small Scale Experimental Study of Vaporization Fluxes of Liquid Nitrogen Released on Water. In: *Symposium Series No. 159, Hazards XXIV*.Vol 159. IChemE; 2014:1-10.

31. Kurihara HM, Myers JE. The effects of superheat and surface roughness on boiling coefficients. *AIChE J*. 1960;6(1):83-91. doi:10.1002/aic.690060117.

32. Bui TD, Dhir VK. Transition Boiling Heat Transfer on a Vertical Surface. *J Heat Transfer*. 1985;107(November):756-763.

33. Basha O, Olewski T, Vechot NL, et al. Modeling of pool spreading of LNG on land. *J Loss Prev Process Ind*. 2014:1-8. doi:10.1016/j.jlp.2014.04.012.

34. Conrado C, Vesovic V. The influence of chemical composition on vaporisation of LNG and LPG on unconfined water surfaces. *Chem Eng Sci*. 2000;55(20):4549-4562. doi:10.1016/S0009-2509(00)00110-X.

35. Collier JG, Thome JR. *Convective Boiling and Condensation*. 3rd ed. (Cullen AL, Woods LC, Brady JM, et al., eds.). Oxford: Clarendon Press; 1994:535-564.

36. Sternling C V., Tickacek LJ. Heat transfer coefficients for boiling mixtures. *Chem Engng Sci*. 1961;16(4):297-337.

37. Lowery AJ, Westwater JW. Heat transfer to boiling methanol-effect of added agents. *Int Engng Chem*. 1957;49:1445-1448.

38. Van Stralen SJD. Heat transfer to boiling binary liquid mixtures Pt. I and Pt. II. *Brit Chem Engng*. 1959;4(1-2):8-17; 78-82.

39. Happel O, Stephan K. Heat transfer from nucleate coiling to the beginning of film boiling in binary mixtures. In: *5th International Heat Transfer Conference*. Tokyo; 1974.

40. Van Stralen SJD, Joosen CJJ, Sluyter WM. Film boiling of water and an aqueous binary mixture. *Int J Heat Mass Transf*. 1972;15:2427-2446.

41. Yue PL, Weber ME. Film boiling og saturated binary mixtures. *Int J Heat Mass Transf*. 1973;16:1877-1887.

42. Mahgerefteh H, Fernandez MI, Harper M, Witlox HWM. An integral model for pool spreading, vaporization and dissolution of hydrocarbon mixtures. In: *Hazards XXIII*. Liverpool, UK; 2012:466-472.

43. Drake EM, Reid RC. How LNG boils on soils. *Hydrocarb Process*. 1975;54(5):191-194.

44. Reid RC, Wang R. The boiling rates of LNG on typical dike floor materials. *Cryogenics (Guildf)*. 1978;18(7):401-404. doi:http://dx.doi.org/10.1016/0011-2275(78)90033-4.

45. Reid RC. *Boiling of LNG on Typical Dyke Floor Materials*. Cambridge, MA; 1980.

46. Takeno K, Ichinose T, Hyodo Y, Nakamura H. Evaporation rates of liquid hydrogen and liquid oxygen spilled onto the ground. *J Loss Prev Process Ind*. 1994;7(5):425-431. doi:10.1016/0950-4230(94)80061-8.

47. Quraishy S. Study of boiling regimes during accidental spill of cryogenic liquids on a solid substrate. 2015.

48. Marshall AL. Cryogenic concrete. *Cryogenics (Guildf)*. 1982;(November):555-565.

49. Dahmani L, Khenane A, Kaci S. Behavior of the reinforced concrete at cryogenic temperatures. *Cryogenics (Guildf)*. 2007;47(9-10):517-525. doi:10.1016/j.cryogenics.2007.07.001.

50. Lentz AE, Monfore G. Thermal Conductivities of Portland Cement Paste, Aggregate, and ConcreteDown to Very Low Temperatures. *J PCA Res Dev Lab*. 1966;8(3):27-33.

51. Drake EM, Jeje AA, Reid RC. Transient boiling of liquefied cryogens on a water surface. II. Light hydrocarbon mixtures. *Int J Heat Mass Transf*. 1975;18(12):1369-1375. doi:10.1016/0017-9310(75)90250-1.

52. *Marine Accident Investigation Report*.; 2014. Available at: http://www.mlit.go.jp/jtsb/eng-mar_report/2014/2013tk0001e.pdf.

53. Lemmon E, McLinden M, Friend D. Thermophysical Properties of Fluid Systems. In: Linstrom P, Mallard W, eds. *NIST Chemistry WebBook, NIST Standard Refernce Database Number 69*. Available at: http://webbook.nist.gov.

54. Canadian Centre for Occupational Health and Safety. 2008. Available at: http://www.ccohs.ca/oshanswers/chemicals/cryogenic/cryogen1.html.

APPENDIX

History of accidents at LNG facilities

Table 8 gives a summary of accidents in the LNG industry.

Table 8: History of accidents at LNG industry [5,6,52]

Year	Place	Cause	Consequence	Additional Information
1944	Cleveland, Ohio, USA	Material failure of the tank walls when exposed to extremely cold temperature of LNG.	LNG vaporized, ignited, exploded and burned 124 fatalities 200-400 injured	The tanks were constructed during world war 2 when metal rationing allowed only 3.5 % nickel construction as opposed to 9% that was required. Tank wall failed when placed in service.
1973	Texas Eastern Company, Staten Island, New York, USA	Use of non-explosion proof equipment despite operating procedure stating otherwise.	Gas trapped in the membrane lined walls ignited. 37 fatalities	The tank was built with membrane lined walls. There was a tear detected and the tank was taken out of service for repair. The workers entered the tank to repair. Ignited gas resulted in fire, which raised the temperature and pressure in the tank that lifted the thick concrete roof and fell on the workers

Table 8: Continued

Year	Place	Cause	Consequence	Additional Information
1979	Lusby, Maryland, USA	LNG leak from LNG pump electrical penetration seal that was improperly tightened. The vapors traveled through the conduit to the substation where a worker switched off circuit breaker.	Gas vapors ignited and caused an explosion at the substation. 1 fatality 1 injured	The substation building design did not include gas detectors as LNG vapors were not expected in the premises. The firms involved in the accident conformed with the regulations and codes. However, this accident led to 3 major changes in the National fire codes.
1985	Pinson, Alabama, USA	Mechanical failure of the patch plate on a vessel containing LNG. The plate propelled to a building with control room, boiler room and offices.	The control room windows imploded and LNG vapors entered the building and ignited. 6 injured	The vessel was being filled with LNG from a liquefaction cold box.

Table 8: Continued

Year	Place	Cause	Consequence	Additional Information
1989	Thurley, UK	LNG entered the vaporizers.	High pressure LNG jet fire. Vapor cloud ignited. Flash fire that burnt the face and hands of 2 operators.	The vaporizers were being cooled to prepare for draining natural gas. One of the drain valves in the vaporizers were not closed before the pumping the natural gas. This led to LNG vapors entering the vaporizer.
2004	Sonatrach LNG liquefaction plant, Skikda, Algeria	Refrigerant line leaked and LNG vapors were drawn into the high-pressure steam boiler.	Boiler exploded damaging other lines that led to larger explosion outside the boiler. 27 fatalities 80 injured	There were three LNG trains that were destroyed. This brought the production for that year to 76% of the normal production.

Table 8: Continued

Year	Place	Cause	Consequence	Additional Information
2014	Near the coast of Singapore	Collision of 216,224 m^3 LNG carrier operated by Qatar Gas Transport Company with 10,114 TEU ship *Hanjin Italy* operated by Hanjin Shipping	No injuries.	No damage to the containment. The vessel's integrity was uncompromised. No pollution risk.
2014	Off the East of Yokohama District of Keihin Port, Japan	Collision of 94,446 tons of LNG tanker *Puteri Nilam Satu* with 2,997 tons LPG tanker *Sakura Harmony*	No casualties.	*Puteri Nilam Satu* received dents and cracks on its hull. *Sakura Harmony* received crushes on its hull.

Description of sensors and devices used in the experimental setup

In this work, the sensors and devices like thermocouples, heat flux sensors, oxygen sensors and ultrasonic anemometer are used and connected to the Data Acquisition (DAQ) system in order to record data and transfer to the computer. The following sub sections describe the sensors and devices used and the associated equations for obtaining the data in engineering units.

Thermocouples

The thermocouples used in instrumenting the experimental setups are ordered from OMEGA. The part number is NMQXL. All the thermocouples used for lab scale experimental setups are type-N with a temperature range from -270 ^{o}C to 1300 ^{o}C. These thermocouples are connected to the DAQ and the signal setup is specified as N28, which is for liquid temperature measurement. This gives the output signal in degree Celsius which is then used for analysis.

Heat flux sensors

The heat flux sensors used in the experimental setups are ordered from OMEGA. Each heat flux sensor is generally provided with an attached calibration certificate that mentions its sensitivity in $\mu V \cdot W^{-1} \cdot m^{-2}$ along with its serial number. These sensors have integrated thermocouple, type-K, for temperature measurements required to calculate heat flux measurements as described below.

The output signal of the heat flux sensors is voltage in mV and temperature in °F. Therefore, the following equation need to be used to get the heat flux value in W m^{-2}.

$$HF = 1000 \cdot \frac{U_{\mathrm{HFS}} \cdot F_{\mathrm{C}}(T)}{S_{\mathrm{HFS}}} \qquad 19$$

where,

HF Heat flux, W m^{-2}

U_{HFS} Output signal (voltage) from sensor, mV

S_{HFS} Sensor sensitivity, µV W^{-1} m^{-2}

F_{C} Correction factor (output multiplication factor which is a function of temperature)

T Temperature read by the sensor, °C

The correction factor, F_{C} is calculated as a function of temperature (in °F) as follows:

$$F_{\mathrm{C}} = \mathrm{A}_1 + \mathrm{A}_2 \cdot T_{\circ\mathrm{F}} + \mathrm{A}_3 \cdot {T_{\circ\mathrm{F}}}^2 + \mathrm{A}_4 \cdot {T_{\circ\mathrm{F}}}^3 + \mathrm{A}_5 \cdot {T_{\circ\mathrm{F}}}^4 + \mathrm{A}_6 \cdot {T_{\circ\mathrm{F}}}^5 \qquad 20$$

where,

A_1 = 1.10

A_2 = $-1.627914 \cdot 10^{-3}$

A_3 = $3.329231 \cdot 10^{-6}$

A_4 = $-6.007836 \cdot 10^{-9}$

A_5 = $-1.592779 \cdot 10^{-11}$

A_6 = $4.987711 \cdot 10^{-14}$

Conversion of degree Celsius to Fahrenheit is calculated using the following equation:

$$°\mathrm{F} = °\mathrm{C} \cdot \frac{9}{5} + 32 \quad (21)$$

Oxygen sensor

The gas detector used to measure the oxygen concentration is ordered from ATESTGAZ (Product code: PW-044-A-SG-X). The range of the detector is 0-25 %v/v. The detector gives the output voltage for oxygen concentration which is converted to concentration units using the following equation:

$$Y\left(\%\frac{v}{v}\right) = \frac{1000 \cdot \Delta Y\left(\%\frac{v}{v}\right)}{16R(\Omega)} X(V) - \frac{\Delta Y\left(\%\frac{v}{v}\right)}{4} \quad (22)$$

where,

Y Oxygen concentration, %v/v

ΔY Range of the device, %v/v

X Voltage output signal, V

R Resistance, Ω

The oxygen concentration, *Y* (in *%v/v*), is converted to number of moles using the density and molar mass of the two components using Equation 23. The mole fraction for each component is calculated using Equation 24.

$$n_i = \frac{V_i \, \rho_i}{MM_i} \quad (23)$$

$$y_i = \frac{n_i}{n_{total}} \quad (24)$$

Where,

n_i Number of moles of component i, moles

n_{total} Total number of moles, moles

V_i Concentration of component i in the vapor phase, %v/v

ρ_i Density of component i, kg m^{-3}

MM_i Molar mass of component i, kmol kg^{-1}

y_i Mole fraction of component i in the vapor phase

The liquid phase composition is calculated using Raoult's law as described in Equation 25. The vapor pressure P_i^{sat} is calculated using Antoine parameters (Table 9) in Equation 26.

$$y_i P = x_i P_i^{sat} \quad (25)$$

$$log_{10}(P_i^{sat}) = A_i - \frac{B_i}{T + C_i} \quad (26)$$

Where,

P Total pressure, bar

P_i^{sat} Vapor pressure of saturated liquid, bar

x_i Liquid mole fraction of component i

A, B, C Antoine parameters for component i

T Temperature of the binary mixture, K

Table 9: Antoine parameter for oxygen and nitrogen [53]

Component	T range, K	A	B	C
Nitrogen	63.14-126	3.7362	264.651	-6.788
Oxygen	54.36-154.33	3.9523	340.024	-4.144

Ultrasonic anemometer

The 3D ultrasonic anemometer used to measure wind velocity at a particular height is ordered from R. M. Young Company (model 81000). This device gives the output voltage for wind speed, wind direction, elevation and sonic temperature. The following are the equations to convert the voltage output signals to meaningful data, Y.

$$Y\left(\frac{m}{s}\right) = 10\left(\frac{m}{s.V}\right) \,.\, \mathrm{X(V)} \qquad 27$$

where,

Y Wind speed, m s^{-1}

X Voltage output signal, V

$$Y(deg) = 108\left(\frac{deg}{V}\right) \,.\, \mathrm{X(V)} \qquad 28$$

where,

Y Wind direction, degrees

$$Y(deg) = 24\left(\frac{deg}{V}\right) \,.\, \mathrm{X(V)} - 60 \qquad 29$$

where,

Y Elevation, degrees

$$Y(°\mathrm{C}) = 20\left(\frac{\mathrm{K}}{\mathrm{V}}\right) \,.\, X(\mathrm{V}) + 220 - 273.15 = 20\left(\frac{\mathrm{K}}{\mathrm{V}}\right) \,.\, X(\mathrm{V}) - 53.15 \qquad 30$$

where,

Y Sonic temperature, °C

Balance

The balance used in the experimental setup is ordered from Mettler Toledo (model MS32001L). This was used to measure the mass loss rate when cryogenic liquid was spilled into the various setups in the laboratory scale experiments. The maximum capacity of the device is 32 kg. It is connected to the computer through a port manufactured by National Instruments and the mass is recorded using a program that is written in LabView.

Data Acquisition (DAQ) system

The Data Acquisition (DAQ) system is a collection of devices such as DBK modules, National Instruments port and Ethernet switch. There are four DBK modules, manufactured by IOtech that were used in the experiments. They are as follows:

- DBK15: This module is used to obtain data from the sonic anemometer and oxygen sensor.
- DBK84: This module is used to obtain data from the heat flux sensors.
- DBK90: This module is used to obtain data from the thermocouples of type N.

All the data from DBK modules are read by DAQView software in the computer.

Calibration of thermocouples

All the thermocouples used in the experimental setups are calibrated to measure the delay in response. This is done to ensure that each temperature reading is accurate. This accuracy is ensured by applying the offsets of each thermocouple from the reference thermocouple. These offsets are calculated during the process of calibration.

Calibration of thermocouples is done at few set temperatures. These temperatures are:

- Boiling point of liquid nitrogen (-196 °C)
- Boiling point of dry ice dissolved in acetone (-78 °C)
- Calibration bath temperatures (-30, -15, 0, +30, +40)

For each of the thermocouples that are used in the experimental setup, three or four set temperatures are used to calibrate them and obtain the offsets. The procedure for calibration are as follows:

- The thermocouples to be calibrated are connected to the DAQ and the channels corresponding to the thermocouples are noted down.
- The reference thermocouple is connected to a reference logging device.
- The DAQ and reference logging device are synced to show the same time.
- To calibrate using liquid nitrogen, a batch of about 10 thermocouples and the reference thermocouple were dipped in liquid nitrogen. To calibrate at -78 °C, they are dipped in a solution of dry ice dissolved in acetone. To calibrate at other temperatures, they are dipped in a heat bath containing silicone oil and the temperature of the bath is set to the calibration temperature.

- Recording is started at the same time for both the DAQ and reference logging device. In the case of calibration using bath, the data is recorded after the temperature of the bath stabilizes to the set value.
- Data is recorded for fifteen minutes.
- The fifteen minute measurements are averaged to give the offset of the thermocouple from the reference temperature. The mean value, median and standard deviation are also calculated.
- The offset function is obtained using Piecewise Cubic Hermite Interpolating Polynomial (pchip) method on MATLAB. This function is then applied to all the temperature measurements taken for each thermocouple used in the experiments.

Concrete surface roughness characterization

There are a total of 6 slabs provided to Texas A&M University at Qatar by LNG training facility (TP-5) at the Ras Laffan Emergency and Safety College (RLESC). These slabs have the same composition of concrete as that used in the building of the large scale setup in RLESC that will be potentially used to conduct future experiments (in the field scale) as an extension to the work done in this thesis. The composition make-up of concrete (provided in Table 3 in Section 5.1) is kept the same for consistency of data collected across different scales.

The surface roughness of both rough and smooth surface concrete bases are measured using surftest SJ 201P/M manufactured by Mitutoyo. The standard specified in

the equipment is JIS B0601-2001, ISO with a sampling length of 8 mm. The equipment is set on "primary profile measurement" mode to obtain the real profile of the surface in terms of average roughness (P_a) for a sample length of 8 mm for each measurement. A total of 20 measurements were taken for rough and smooth surface each. Table 10 provides the sample data collected for rough surface. The average of the 20 measurements gave the average roughness of the complete surface that is provided in Table 4.

Table 10: Surface roughness measurements for rough concrete

No.	Pa (μm)
1	41.25
2	37.02
3	34.81
4	45.53
5	41.72
6	35.27
7	45.35
8	41.23
9	40.15
10	46.35
11	38.93
12	39.97
13	41.37
14	30.51
15	48.43
16	30.76
17	38.06
18	40.98
19	32.84
20	45.62
Average	39.81
Median	40.57
St. Dev.	5.13
St. Dev., %	0.13

Sensor locations in experimental setups

Figure 35: Experimental setup for rough surface concrete base in the lab

Table 11: Sensor location in the rough and smooth surface concrete base setups

Thermocouple locations			
Thermocouples	x (mm)	y (mm)	z (mm)
T1	73.0	199.0	50.0
T2	112.0	105.0	50.0
T3	180.0	220.0	50.0
T4	196.0	174.5	50.0
T5	204.5	44.5	50.0
T6	56.0	188.0	0.0
T7	95.0	94.0	0.0
T8	187.5	33.5	0.0
Heat flux sensor locations			
Heat flux sensors	x (mm)	y (mm)	z (mm)
H1	250.0	0.0	80.0
H2	147.0	133.0	50.0
H3	130.0	122.0	0.0

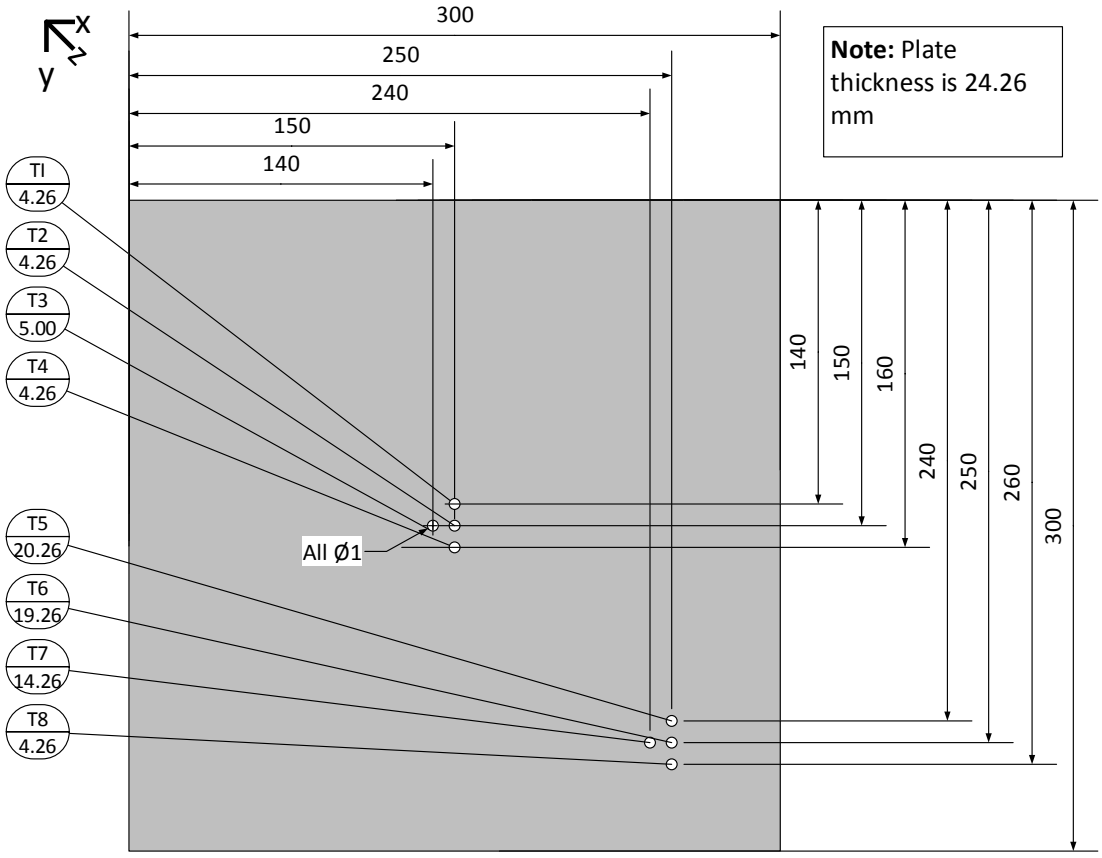

Figure 36: Engineering drawing of Steel base set up - bottom view where the depth is mentioned below the thermocouple label (All dimensions mentioned in mm)

Table 12: Sensor location in the steel base setup

Thermocouple locations			
Thermocouples	x (mm)	y (mm)	z (mm)
T1	150.0	140.0	4.3
T2	150.0	150.0	4.3
T3	140.0	150.0	5.0
T4	150.0	160.0	4.3
T5	250.0	240.0	20.3
T6	250.0	250.0	19.3
T7	240.0	250.0	14.3
T8	250.0	260.0	4.3
T9	56.0	188.0	0.0
T10	95.0	94.0	0.0
T11	187.5	33.5	0.0
Heat flux sensor locations			
Heat flux sensors	x (mm)	y (mm)	z (mm)
H1	250.0	0.0	80.0
H2	130.0	122.0	0.0

Table 13: Sensor location in the polystyrene base setup

Thermocouple locations			
Thermocouples	x (mm)	y (mm)	z (mm)
T1	170.0	220.0	148.0
T2	230.0	200.0	148.0
T3	100.0	200.0	100.0
T4	170.0	180.0	100.0
T5	230.0	220.0	100.0
T6	170.0	180.0	50.0
T7	230.0	220.0	50.0
T8	300.0	200.0	50.0
T9	230.0	180.0	2.0
T10	50.0	200.0	200.0
T11	100.0	200.0	170.0
T12	100.0	210.0	155.0
T13	148.0	180.0	155.0
T14	252.0	210.0	200.0
T15	252.0	220.0	170.0
T16	300.0	230.0	200.0
T17	350.0	200.0	155.0
Heat flux sensor locations			
Heat flux sensors	x (mm)	y (mm)	z (mm)
H1	180.0	210.0	100.0
H2	180.0	210.0	50.0
H3	300.0	180.0	170.0

Risk analysis for liquid nitrogen and liquid nitrogen/oxygen mixture

Risk matrix and acceptance criteria

The categories of the severity of the consequence and the probability utilized in this work are in Table 14 and Table 15. Risk matrix used is shown in Figure 37 and the acceptance criteria of the risk are summarized in Table 16.

Table 14. Likelihood of the event

Likelihood (L)	Category	Description	Likelihood as function of number of barriers
Frequent	A	Likely to occur frequently or continuously experienced.	No barriers; or only one Administrative or PPE
Probable	B	Will occur several times during life cycle	Only one Engineering; or combination of no more than two Administrative or PPE
Occasional	C	May occur sometime, but rather rarely	Only one Engineering and at least one Administrative or PPE; or at least three Administrative or PPE Barriers

Table 14: Continued

Likelihood (L)	Category	Description	Likelihood as function of number of barriers
Remote	D	Unlikely, but possible to occur	At least two Engineering Barriers; or one Engineering, good inherently safer design, and at least one Administrative or PPE
Improbable	E	So unlikely that it can be assumed it will not occur	At least two Engineering Barriers, good inherently safer design and some administrative or PPE

Table 15. Severity of the consequences

Severity (S)	Category	Description	Examples
Catastrophic	1	Death, life-threatening health effects, permanent serious disability. (Irreversible significant environmental impact or catastrophic damage to asset)	Death or paralysis. Leg or hand amputation.
Critical	2	Permanent partial disability, severe injury or illness that may result in long hospitalization or serious health effects that could impair the ability to take protective action. (Reversible significant environmental impact. Extensive damage to asset.)	A deep burn or a major broken bone. Asphyxiation.

Table 15: Continued

Severity (S)	Category	Description	Examples
Moderate	3	Mild, transient health effects, injury or illness resulting in more than one lost work day and which may require some hospitalizing, but rather short. (Reversible moderate environmental impact. Minor damage to asset.)	Small burn. A broken finger or toe.
Marginal	4	Minor injury: injury or illness resulting in no more than one lost work day. (Minimal environmental impact or asset damage.)	A small cut or twisted ankle.

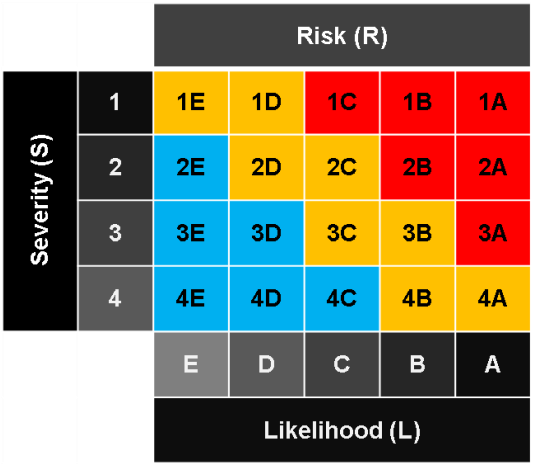

Figure 37: Risk Matrix

Table 16. Risk acceptance criteria

Acceptable Risk (blue)	**Tolerable Risk (yellow)**	**Unacceptable Risk (red)**
Medium to low risk, which is fully acceptable with periodic review and control.	Serious risk, which is tolerable, if demonstrated that is controlled and reduced to ALARP. Make changes if possible.	High risk, which is not acceptable at any time. Do not Operate. Apply risk reduction measures.
Inspect annually	**Inspect monthly**	**Inspect daily until corrected**

Hazard identification

The hazard identification is carried out using What-if Analysis as shown in

Following abbreviations are used in the analysis:

LN2 - liquid nitrogen

LO2 - liquid oxygen

LN2/LOX - liquid nitrogen/oxygen mixture

Table 17: What-if Analysis

No.	Hazard	Causes	Consequences	Safeguards	S	L	R
1	Gas (in case of LN2 only) that displaced oxygen and leads to asphyxiation	Mechanical damage of the LN2 cylinder	Spill of large LN2 quantity. Difficulty in breathing or asphyxiation (depending on size of the spill and concentration). May be catastrophic only if occurs in small, not well ventilated space/room (like an elevator)	Dewar has specially designed wheels for transportation. Dewar has double walls. Transport small Dewar with care. Two persons have to transport a full Dewar. No other persons are allowed in the elevator (please ask them to not enter and take another one or wait)	2	D	2D

Table 17: Continued

No.	Hazard	Causes	Consequences	Safeguards	S	L	R
2	same as above	Large LN2 quantity release due to overpressure (see # 7)	Burst of the cylinder or catastrophic rupture of the pressurized cryogenic liquid cylinder. Spill of large LN2 quantity. Difficulty in breathing or asphyxiation (depending on size of the spill and concentration). Potential pressure wave and flying objects.	Pressure Relief Valve (see also #7) Rupture disc. Perform experiment in well-ventilated area (near to an open fume hood) or under fume hood.	1	D	1D

Table 17: Continued

No.	Hazard	Causes	Consequences	Safeguards	S	L	R
3	same as above	Spill during the refill of the small container	Difficulty in breathing or asphyxiation (depending on concentration) - only within close proximity of setup	Work performed with small liquid quantity only – less than 2 litre. Tray below the box to contain spills. Perform experiment in well-ventilated area (near to an open fume hood) or under fume hood. Do not stay near the test box unless necessary.	1	E	1E

Table 17: Continued

No.	Hazard	Causes	Consequences	Safeguards	S	L	R
4	Hot surface of heater (only used for concrete and steel pads)	The heater is designed to operate at high temperature (up to 981□C)	Burn of hand, when touched. Walls' polystyrene may melt	Experiment is designed to set maximum temperature to 100 deg.C only. Switch-off button on the control box of the heater. Switch-off on the main power cable (next to big blue plug). Experimental setup is designed in such a way that touching hot surface is difficult. Wait and allow the surface to cool down before touching any parts of the heater. Wear high temperature or leather gloves if necessary.	3	D	3D

Table 17: Continued

No.	Hazard	Causes	Consequences	Safeguards	S	L	R
5	Cryogenic liquid - temperature	A contact of bare body to the vessel that contain cryogenic liquid (excluding Dewar) - human error	Cold burn of relatively small part of body (as vessel is small)	Experiment is design to be small: small box and small liquid quantity. Wear cryogenic PPE (apron and gloves) when dealing with cryogenic liquids. Wear long sleeve or lab coat and long legs. Two people working during refill.	4	D	4D

Table 17: Continued

No.	Hazard	Causes	Consequences	Safeguards	S	L	R
6	same as above	Spill of cryogenic liquid on bare body - direct contact with cryogenic liquid	Cold burn of relatively small to moderate part of body (as liquid quantity is small)	Work performed with small quantity only – less than 2 litre. Transport small Dewar with care in designed small Dewar or cryogenic vessel. Tray below the box to contain spills. Wear cryogenic PPE (apron and gloves) when dealing with cryogenic liquids. Wear long sleeve or lab coat and long legs. Wear closed shoes that do not soak or allow liquid to contact foot. Emergency shower available.	3	E	3E

Table 17: Continued

No.	Hazard	Causes	Consequences	Safeguards	S	L	R
7	Overpressure in pressurized cryogenic liquid cylinder	Cylinder exposed to excessive heat due to external fire	Vapor release through the pressure relieve valve (full cylinder burst covered in #2). Potential asphyxiation.	Do not expose to excessive heat, do not store near flammable liquids. Fire detectors and sprinklers - general building alarm. Oxygen gas detector in the lab.	2	E	2E
8	same as above	same as above	Same as #2.	Same as #2.	See #2 for risk estimation		

Table 17: Continued

No.	Hazard	Causes	Consequences	Safeguards	S	L	R
9	Electric shock from the Data Acquisition System	Damaged electrical connections at high (240V) voltage side (leads/cables, elements of the electronics rack and power supply). Operator touch high voltage wires inside the (240V) voltage box once not switch off.	Electric shock. Potential for serious injury or death.	Good housekeeping practice to ensure that cables are placed away from sources of heat or water as well as are not exposed to abrasion. User must not open (240V) voltage box when power supply is on. Always switch off power and always disconnect the power cable from the wall before you open high (240V) voltage box of data acquisition DAQ system The electronics rack and power supply should be switched off when connecting sensor cables. The high (240V) voltage box is closed and key are with PI or authorised senior lab person DAQ rack is grounded and fuse protected.	1	E	1E

Table 17: Continued

No.	Hazard	Causes	Consequences	Safeguards	S	L	R
10	Electric shock from the Heater	Damaged electrical connections at high (240V) voltage side (leads/cables, elements of the electronics rack and power supply). Operator touch high voltage wires inside the (240V) voltage box once not switch off.	Electric shock. Potential for serious injury or death.	Good housekeeping practice to ensure that cables are placed away from sources of heat or water as well as are not exposed to abrasion. The cable is strong and has special shield/insulation that is resistant to abrasion. User must not open (240V) voltage box when power supply is on. Always switch off power and always disconnect the power cable from the wall before you open high (240V) voltage box of the heater. Heater control box is grounded and fuse protected.	1	D	1D
11	Trip over cable and fall	Disorganized cables	Fall and injuries that may vary from minor to serious or even death (if hit head by sharp edge) - here minor (see below)	Good housekeeping practice to ensure that cables are tidy to avoid trip hazards Rubber, no-easy-slip shoe sole is recommended Regular inspections by students, research staff and faculty	4	C	4C

Table 17: Continued

No.	Hazard	Causes	Consequences	Safeguards	S	L	R
12	same as above	same as above	Fall and injuries that may vary from minor to serious or even death (if hit head by sharp edge) - here major (see above)	Good housekeeping practice to ensure that cables are tidy to avoid trip hazards Rubber, no-easy-slip shoe sole is recommended Regular inspections by students, research staff and faculty Frequency reduced by conditional event (the person must hit very bad to die)	1	D	1D

Table 17: Continued

No.	Hazard	Causes	Consequences	Safeguards	S	L	R
13	Higher concentration of liquid oxygen in the cylinder	Mixture of LAIR kept for long period and oxygen concentration increase due to preferential boiling of liquid nitrogen	Pure or higher LOX concentration is possible in the miture. No consequences to the equipment. Flammability limits of the liquid vapors may change if present, some chemicals may ignite in oxygen if they exposed, both of which may lead to fire. Potentially we may spill pure LOX into experimental setup, but it has no negative consequences.	Dewar is designed to hold pure LOX with no consequences. Organic materials or sensitive chemicals are stored away from the Dewar. Small quantity is spilled during the experiment, which will not significantly change oxygen concentration outside of experimental setup. Fire extingusher available in case of fire. Laboratory fire detection and sprinkler system. Always two persons present during the experiment.	3	E	3E

Checklist for the experiments

Table 18: Checklist before the experiment

Action	Confirm status	Comments
Review, update and sign HAZID, PSA and SOP		
Make sure the setup of the experiment is done and complete		
Make sure all sensors are connected. Verify channels associated.		
Copy the heat flux serial number from labels in RLIC to \P: drive.		
Measure all dimensions of experiment, location of all sensors, etc.		
Take pen drives to take back up of data		
Inform other people in the lab about the experiment timing – Time and duration		
Check Ethernet connection (DAQ<->Hub, NI-RS232<->Hub, Hub<->Computer)		
Make sure wireless internet switch is off on the laptop		
Prepare LabView file		
Run NI-serial troubleshooter (inside folder "NI-serial" on desktop) and note the COM number to which the balance is connected		
Run "Balance" program		
Set proper COM number		
Make sure proper time interval (sampling rate)		
Tare Balance (without box) and note down the weight of the box		

Table 18: Continued

Action	Confirm status	Comments
Tare balance with box		
Click “Start Acquiring”		
Setup file name and location		
Check if the data is recording		
Prepare DaqView file		
Switch on DAQ		
Run DAQView		
Device -> configure hardware setting		
Select external connection corresponding to P1 channels that are connected -> OK		
Select “On” column -> Set “Channel ON” to “No”		
Select “Ch” that are connected and set “Channel ON” to “Yes” (set all CJC of thermocouples to “Yes”		
Click “Hide INACTIVE Channels”		
File->save as->tamuq data folder		
Acquisition setup tab->Set “trigger event” to “immediately” and “stop event” to “Manual stop” and set scan rate as 1 s		
Data destination->file name: *.bin->base directory: browse to saved file		
Click “File conversion preferences” and ALWAYS have “ASCII text” checked and “Add timestamp to ASCII text files” checked		
Run and make sure no error shows on the Ch		
Click “Acquire”		

Table 18: Continued

Action	Confirm status	Comments
Prepare description of files		
record the time of starting all files		
record general description of setup and experiment		
Prepare camera and camcorder		
synchronize time of cameras with computer		
synchronize time of your watch with computer		
set up and start video camera (camcorder)		
List of things to do on the day of experiment		
Take video of entire experiments		
Check values in DAQ after end of each run		
Take copies of data recorded in DAQ		